University of Texas at Arlington

MavMatrix

2023

An Investigation of Peak Shape Models in Chiral Separations

Ryan Jacob Burk

Follow this and additional works at: https://mavmatrix.uta.edu/chemistry_theses

Part of the Chemistry Commons

Recommended Citation

AN INVESTIGATION OF PEAK SHAPE MODELS IN CHIRAL SEPARATIONS

By

Ryan Jacob Burk

Presented to the Faculty of the Graduate School of

The University of Texas at Arlington in Partial Fulfillment

of the Requirements for the Degree of

MASTER OF SCIENCE IN CHEMISTRY

THE UNIVERSITY OF TEXAS AT ARLINGTON

May 2023

Supervising Committee:

Dr. Daniel W. Armstrong, Supervising Professor

Dr. Saiful Chowdhury

Dr. Fred MacDonnell

Acknowledgement

I would like to express my gratitude to my research advisor, Dr. Daniel W. Armstrong, for his guidance and support throughout my research and studies. His knowledge and experience have been invaluable in my journey to success, and I feel fortunate to have had the opportunity to work under his leadership. I would also like to extend my heartfelt thanks to Dr. M. Farooq Wahab, who has been an indispensable source of help and support throughout all stages of my research. From practical tasks such as instrumentation training to programming and editing of written materials, Dr. Wahab's expertise and generosity have been a constant source of motivation. I am also grateful to my committee members, Dr. Chowdhury and Dr. MacDonnell, for their valuable time and feedback. I would also like to thank AZYP, LLC (Arlington, TX) for providing the core shell particles and columns for this research. Finally, I would like to acknowledge my fellow group members for their support throughout this project.

Abstract

AN INVESTIGATION OF PEAK SHAPE MODELS IN CHIRAL SEPARATIONS

Ryan Burk, MS

The University of Texas at Arlington, 2023

Supervising Professor: Daniel W. Armstrong

The use of superficially porous particles in chromatography has led to significant improvements in separation efficiency. However, peak asymmetry in enantiomeric separations causes performance comparisons across particle types a challenge. In this study, we screened 28 pharmaceutically relevant compounds and developed practical methods to reduce peak asymmetry in normal phase chiral chromatography. The use of additives was found to be effective in reducing peak tailing for all compounds, including neutrals. Additionally, we observed that solvent mismatch with the eluent can cause system peak interference, which can be managed by reducing injection volumes. To more accurately assess the performance of the separations across the two column types, mathematical models that accounted for peak shape distortions were applied. After minimizing these distortions, we found that the SPP column had more efficient kinetics than the FPP column, despite the latter performing better in some separations. Our findings highlight the importance of optimizing peak shape in enantiomeric separations to achieve accurate and reliable results.

Table of Contents

List of Illustrations

List of tables

1. Introduction

The term chirality refers to mirror-image, non-superimposable molecules[1]. The International Union of Pure and Applied Chemistry (IUPAC) definition of chirality is "the geometric property of a rigid object (or spatial arrangement of points or atoms) of being non-superposable on its mirror image; such an object has no symmetry elements of the second kind (a mirror plane, $\sigma=S_1$, a centre of inversion, $i=S_2$, a rotation-reflection axis, S_{2n}). If the object is superposable on its mirror image the object is described as being achiral" [2]. The experimental difference between chiral molecules is their optical activity [3].

Prior to the 1980s, pharmaceutical companies paid little attention to chirality and compounds were synthesized and sold as racemates. However, this idea was challenged with the distribution of a drug called thalidomide. Thalidomide was a sedative intended as medication for anxiety or insomnia. This now infamous drug caused severe deformities in children if taken by pregnant mothers. It is estimated that more than 10,000 children were born with severe congenital disabilities as a result of thalidomide as well as increased rates of miscarriages [4]. It is now believed that only the *S*-enantiomer of thalidomide resulted in birth defects [5]. The U.S. Food and Drug Administration (FDA) passed new guidelines for the development of chiral pharmaceutics in 1992 [6]. Since then, the need for effective chiral separations has become essential for the development of many pharmaceutical products.

Since modern FDA guidelines have made chiral chromatography of critical interest for the development of drugs, many chiral stationary phases (CSP) have been developed to cover a variety of compounds and chromatographic modes such as π-complex, macrocyclic bonded stationary phases, macrocyclic glycopeptides, and polysaccharide chiral stationary phases to name a few [3]. Π-complex CSPs are compounds with functionalized aromatic hydrocarbons. These CSPs depend on π-π stacking, dipole interactions and/or H-bonding with the analyte. Macrocyclic bonded CSPs are cyclic chiral selector of moderate mass bonded to structural supports. An example of this would be chiral crown ethers or cyclodextrins which are capable of making inclusion complexes with certain enantiomers [7]. Macrocyclic glycopeptides are CSPs of moderate molecular masses ranging from 600 to 2200 Daltons consisting of structures containing a glycosylated cyclic or polycyclic non-ribosomal peptides [3]. These CSPs tend to have a large number of stereogenic centers to increase chiral recognition. Such macrocyclics are obtained from fermentation processes. Vancomycin and teicoplanin are examples of macrocyclic glycopeptide chiral selectors. Finally, derivatized cellulose and amylose CSPs, known as polysaccharide CSPs, show effectiveness for a wide variety of enantiomers. It has been proposed that the chiral helical structure of the cellulose and amylose polymers are responsible for their chiral selectivity [8]. The availability various of CSPs and selection mechanisms poses important considerations in the chiral screening process.

For a chiral selector to be effective, a minimum of three points of interaction are required with at least one of the enantiomers [9, 10]. These interactions can consist of

2

any variety of attractive or repulsive intermolecular forces. Chiral recognition could come from even a single associative interaction with two repulsive interactions as long as the associative interaction is stronger than the combined repulsive interactions [11]. Often stronger forces such as ionic interactions are primarily involved in achiral binding, while weaker interactions such as hydrogen bonds, π-π interactions, and steric repulsive interactions are more responsible for chiral separations [12].

Brush-type chiral selectors are a class of chiral selectors used in chiral chromatography that have a flexible, dendritic structure capable of a least two conformational states [13]. These chiral selectors consist of a central core structure with multiple branches that extend outward. The branches typically contain chiral or achiral groups that can interact with the enantiomers of the analyte to be separated. The dendritic structure of brush-type chiral selectors provides a high density of interaction sites, which can lead to efficient chiral recognition and separation. Brush-type CSPs are ideal candidates for enantioselective HPLC because they are easily reproducible [14]. One of the best-known brush-type CSPs is the Whelk-O, a π-π CSP that was originally developed by Pirkle et al. for the separation of naproxen [15]. Since then, it has proven to be an effective stationary phase for pharmaceutically relevant compounds such as anti-inflammatory or antiepileptic drugs [16, 17]. The structure of Whelk-O 1 (S, S) can be seen in Figure 1.
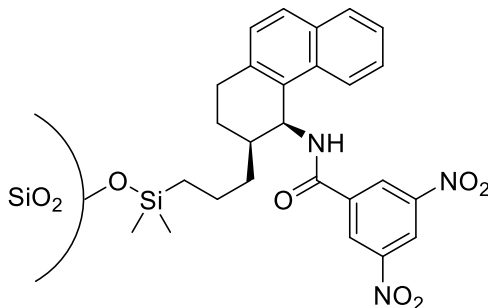
Figure 1. Structure of Whelk-O 1 (*S, S*) chiral selector

It has been proposed that the three points of interaction on Whelk-O (*S, S*) are the tetrahydrophenanthrene and dinitrobenzamide π-systems and the amide hydrogen bonding site [3]. Π-π interactions are stronger in the normal phase mode of chromatography [18]. Sub/supercritical fluid chromatography (SFC) uses "greener" mobile phases, so it is extremely attractive for industrial or preparative scale separations. Because normal phase separations can be easily translated to SFC, normal phase conditions on the analytical scale have been chosen in this work for screening purposes. Additionally, the (*S, S*) form was selected for examination because it is commercially available on superficially porous particles. Superficially porous particles (SPPs) as the support material can further enhance the efficiency of the separation. SPPs have a lower surface area than fully porous particles and can provide faster mass transfer kinetics, resulting in reduced band broadening and higher efficiency [11, 19, 20].

In 1941, Martin and Synge defined a system of evaluating the separation efficiency by the number of theoretical plates, N, where each plate represents an analyte equilibrium step between the mobile and stationary phases [21]. The number of

theoretical plates can be calculated using equation 1-1 where t_r is the retention time, and w is the width of the peak at the base. The height equivalent to a theoretical plate, H, is found by dividing the column length, L, by the number of plates (equation 1-2). In 1954, van Deemter et al. derived a mathematical relationship between solvent linear velocity through a column and H which has since become the most widely used system of analyzing band broadening [22]. The van Deemter expression can be seen in equation 1-3, where the height equivalent to a theoretical plate (*H*) is the sum of band broadening by eddy diffusion (*A*), longitudinal diffusion (*B*), and mass transfer (*C*) as a function of the linear velocity of the mobile phase (*u*).

$$N = 16\frac{t_r{}^2}{w^2} \tag{1-1}$$

$$H = \frac{L}{N} \tag{1-2}$$

$$H = A + \frac{B}{u} + Cu \tag{1-3}$$

However all of these aforementioned expressions require idealized Gaussian behavior that often inadequately predicts the true chromatographic behavior [23]. As result, many of these equations need to be adapted for less optimal conditions. An example is to use peak width at half height, $w_{1/2}$, to calculate N as seen in equation 1-4, if the peaks are poorly resolved [24]. Additionally, for peaks that do not fit the Gaussian model well, equation 1-5 can be used to calculate theoretical plates from peak moments where m_1 and m_2 are the first and second moments respectively [25]. The statistical

moment analysis method is, in fact, the most accurate, "gold standard" method [25].

Equations 1-1 and 1-4 are derivations of the statistical moment method if the peak fits a

Gaussian distribution. In essence, the more common method of analyzing efficiency

assumes a Gaussian peak model in the majority of commercial chromatographs.

$$N = 5.54 \frac{t_r^2}{w_{1/2}^2} \qquad (1\text{-}4)$$

$$N = \frac{m_1^2}{m_2} \qquad (1\text{-}5)$$

When analyzing a chromatographic separation, it is often valuable to apply a

peak model. Peak models are particularly valuable when peaks are not baseline

resolved. Unfortunately, it is common for peaks to show a degree of overlap with

neighboring peaks and peak asymmetry [26-28]. A peak model provides a practical

method for analyzing a peak in a separated mixture as though it were in isolation.

Additionally, peak models detail the peak with a completely smoothed baseline. A

smoothed baseline is particularly valuable when signal noise is causing interference in

the analysis of a separation. These peak models provide useful approximations of the

real chromatographic peak, which can then be used for performance evaluations such as

efficiency or selectivity. A variety of models are regularly applied to fit peaks, so it can

be important to consider the strengths of each when modeling a desired peak.

One such approach is the Gaussian function which models as a normal

distribution. This model is highly symmetric and encountered in virtually all fields of

experimental science. The equation of a Gaussian peak can be seen in equation 1-6 where m_0 is the zeroth moment which represents peak area (1-7), m_1 is the first moment which is equivalent to the mean value of the peak (1-8), m_2 is the second moment which is the peak variance (1-9), t is time, and S is the signal. In ideal conditions, the analyte is expected to fit the Gaussian distribution perfectly, however, real chromatographic peaks are subjected to a variety of effects that cause it to deviate from the normal distribution [29].

$$y(t) = \frac{m_0}{\sqrt{2\pi m_2}} e^{-\frac{1}{2}(\frac{t-m_1}{m_2})^2} \tag{1-6}$$

$$m_0 = \int_{t1}^{t2} y(t)dt \tag{1-7}$$

$$m_1 = \frac{\int_{t1}^{t2} ty(t)dt}{m_0} \tag{1-8}$$

$$m_2 = \frac{\int_{t1}^{t2}(t - m_1)^2 y(t)dt}{m_0} \tag{1-9}$$

A more sophisticated method for modeling is to apply a convolution model. In these cases, a Gaussian model is convolved with a broadening function that can better account for various broadening effects on real chromatographic separations. The exponentially modified Gaussian function (EMG) convolves a truncated exponential decay function to better account for extra-column band broadening. A degree of asymmetry as a result of extra-column effects is expected in nearly all separations which made EMG an effective model for a majority of chromatographic peak shapes. The

equation for bidirectional (tailing as well as fronting) EMG can be seen in equation 1-10

where A is the peak area, σ is the standard deviation of the pre-distorted Gaussian, μ is

the mean of the Gaussian, and τ is a distortion parameter that describes the tailing of

the peak [30]. Similarly, the Gaussian modified Gaussian (GMG) is a convolution model

that distorts the normal distribution with a half-Gaussian function. The GMG function

can be seen in equation 1-11. This model becomes more asymmetric as the width of the

half-Gaussian response is increased. The GMG model was developed to account for

intracolumn band broadening effects [31]. GMG is also capable of accounting for

fronting in addition to tailing, although it does not describe extra-column broadening as

well as EMG does. These models are necessary for chiral chromatography because peak

asymmetry is particularly common for enantiomeric separations [25].

EMG,
$$y(t) = \frac{A}{2\tau} \exp\left(\frac{\sigma^2}{2\tau^2} + \frac{\mu - t}{\tau}\right) \left[\mathrm{erf}\left(\frac{t - \mu}{\sqrt{2}\sigma} - \frac{\sigma}{\sqrt{2}\tau}\right) + \frac{\tau}{|\tau|}\right]$$
(1-10)

GMG,
$$y(t) = \frac{A \exp\left(-\frac{1}{2}\frac{(x - \mu)^2}{\tau^2 + \sigma^2}\right)\left[1 + erf\left(\frac{\tau(t - \mu)}{\sqrt{2}\sigma\sqrt{\tau^2 + \sigma^2}}\right)\right]}{\sqrt{2\pi}\sqrt{\tau^2 + \sigma^2}}$$
(1-11)

The interactions responsible for some enantiomeric separations exhibit much

slower adsorption/desorption kinetics when compared to achiral interactions which

commonly result in peak tailing [12, 32, 33]. In addition to these kinetics, peak shapes

can also be distorted by factors other than the analyte such as extra-column tubing, the

detector sampling rate, or column packing.[25, 34]. These broadening effects tend to

create peaks that are more accurately represented by the Langmuir model rather than

Gaussian which changes the peak's moments. Gaussian models are still most commonly applied to fit asymmetric peaks which have been shown to overestimate theoretical plates and van Deemter performance [35, 36].

In this work, 28 compounds are screened for enantiomeric separation on Whelk-O (*S,S*) columns for peak shape analysis. The performance results from a 2.7 μm superficially porous (SPP) column are compared to 5 μm fully porous column (FPP). It is expected that smaller core-shell particle packing will increase efficiency by narrowing and sharpening the peaks. [37-39]. This change is explained by the core-shell particles having smaller diameter as well as having a narrower size distribution which reduces eddy diffusion [37]. Additionally, broadening from longitudinal diffusion is reduced because the effective column volume is reduced [39]. The kinetic advantages of the SPP column can be seen by representing the van Deemter data as a kinetic plot which plots the peak efficiency on the x-axis and the dead time on the y-axis.

In addition, the effects of additives and sample solvents on peak shape are examined. Mobile phase additives can cause significant changes to the shape of the peak that render some models significantly less accurate than others. Similarly, sample solvent also can create disturbances known as system peaks that can result in deformities in peak shape [40]. This work compares how these effects create model-dependent differences that can be seen in the van Deemter curves.

2. Experimental methods

All enantiomeric compounds were obtained from MilliporeSigma (MO, USA) and Alfa

Aesar (MA, USA). Sulfinpyrazone was obtained from Fluka Analytical (TX, USA). Ethotoin

was obtained from Enamine (OH, USA). Etodolac was obtained from Matrix Scientific

(SC, USA). Hexanes (F.W. 86.18 g/mol; d= 0.673 g/mL at 25 °C) was purchased from

Fisher Chemical (MA, USA). Ethanol 200 proof (F.W. 46.1 g/mol; d = 0.787 g/mL at 25 °C)

was purchased from Decon Laboratories, inc (PA, USA). Acetic acid (F.W. 60.05 g/mol;

d= 1.049 g/mL at 25 °C), trifluoroacetic acid (F.W. 114.02 g/mol; d= 1.489 g/mL at 25 °C),

and triethylamine (F.W. 101.19 g/mol; d=0.726 g/mL at 25 °C) were obtained from

MilliporeSigma (MO, USA). 18 MΩ distilled water was purified on-site by a Thermo

Scientific GenPure Pro UV purifier.

(S,S)-WhelkoShell columns (5 or 10 cm x 4.6 mm i.d., 2.7 μm SPP) were provided by

AZYP LLC (TX, USA). (S, S)- Whelk-O 1 Kromasil columns (5 or 10 cm x 4.6 mm i.d., 5 μm

FPP) were gifted from Regis Technologies, Inc (IL, USA) Batch #M24745-1040-4. All

chromatographic separations were done using an Agilent 1220 series LC equipped with

a quaternary pump (G1311A), autosampler (G1367C), thermostat (G1316B), and D2

detector (G1315B). Degassing was done manually using an Aquasonic (Model 250 HT)

ultrasonicator from VWR Scientific Products. Enantiomeric separations for comparison

of 10 cm SPP particle to FPP particle columns were done at ambient temperature. The

temperature was maintained at 25 °C for van Deemter experiments using 5 cm columns

of the same packing material. All stationary phases are bonded with (S,S) Whelk-O 1 as the chiral selector.

Mobile phases were prepared manually with class A 500 mL graduated cylinders. Additives were added to mobile phases using micropipette purchased from Ward's Science. Mobile phase concentrations are reported as percent by volume. For example, a 1000 mL 20/80/0.3/0.2 ethanol/ hexanes/ acetic acid/ triethylamine would be made by mixing 200 mL of 200-proof ethanol with 800 mL of hexanes. 3 mL of acetic acid and 2 mL of triethylamine would be delivered using a micropipette. The mobile phase would be mixed manually and degassed in the ultrasonicator.

Efficiency calculations for the Gaussian model were calculated with the Agilent onboard software using the peak width at half-height method. Peaks were modeled and analyzed using Peakfit v4.12.00. from Seasolve. Chromeleon 7 Chromatography Data System Software by Thermo Scientific was used for statistical moment analysis.

3. Results and Discussion

3.1. Constant mobile phase conditions comparison. Previous reports have demonstrated that SPP outperforms FPP when translated to chiral separations in terms of efficiency and speed. This observation holds even when FPP particles have smaller diameters than the SPP particles [11]. However, Gasparrini et al. claimed that the value of SPP does not translate for enantiomeric separations in all cases [19]. Variables that impact peak shape and efficiency analysis must be better resolved to further understand the effects of SPP on normal phase chiral chromatography. A screening library was

11

compiled for pharmaceutically relevant compounds in this work. A full list of compounds

is shown in Table 1. The enantiomers were separated on a 10 cm x 0.46 cm i.d. column

with 2.7 µm SPP using Whelk-O as a chiral selector. The same samples were then

separated using a 10 cm x 0.46 cm i.d. column with 5 µm FPP of the same selector.

Separations on both columns were run isocratically with the same mobile phase
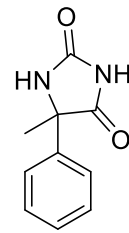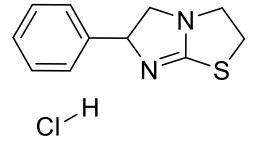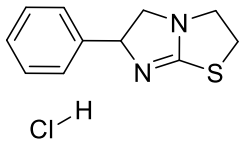
compositions, so this is referred to as constant mobile phase mode.
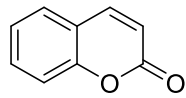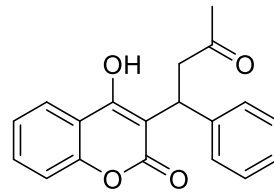
Troger's Base
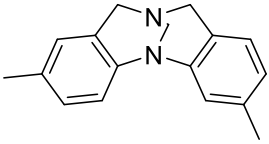
Carprofen
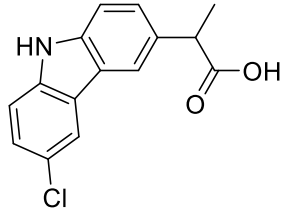
5-methyl-5-phenylhydantoin

Tetramisole

Naproxen
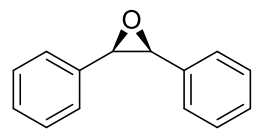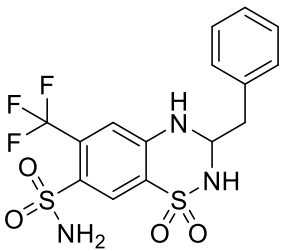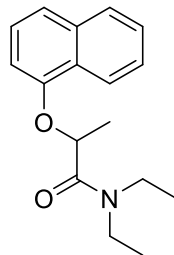
Coumarin

Warfarin

Trans-stilbene oxide

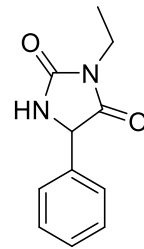Bendroflumethiazide
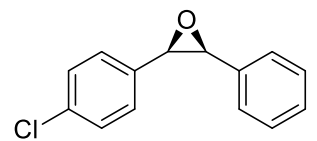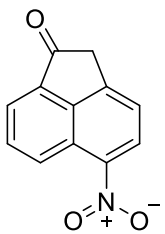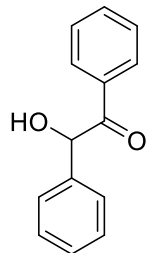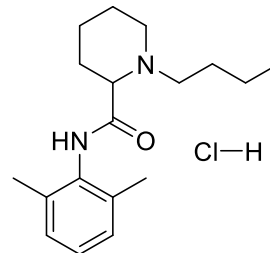
Devrinol

Ethotoin

Trans-chlorostilbene oxide

1-acenaphthenone
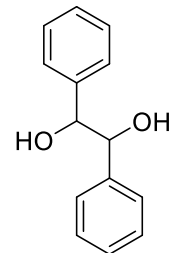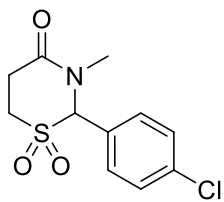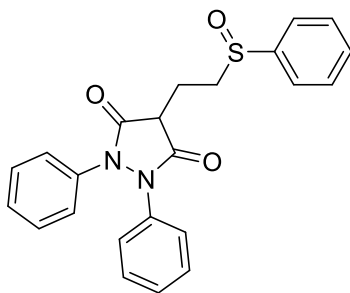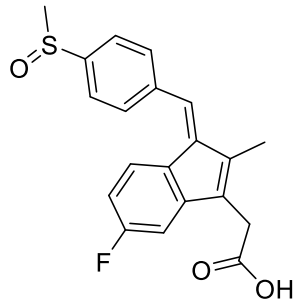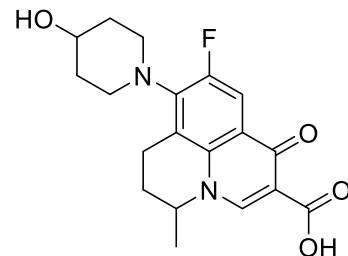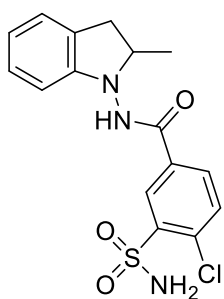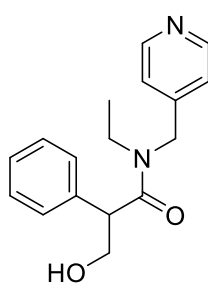
Benzoin

Bupivacaine

Hydrobenzoin

13

Chlormezanone

Sulfinpyrazone

Sulindac

Nadifloxacin

Indapamide

Tropicamide

Oxazepam
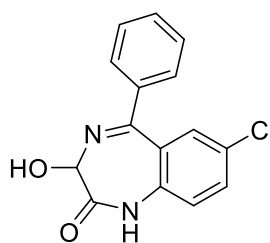
Ibuprofen
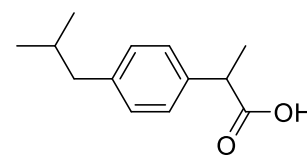
Ketoprofen
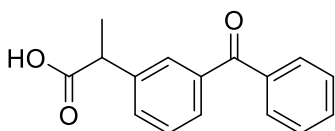
Flurbiprofen
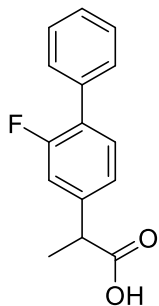
Nimodipine
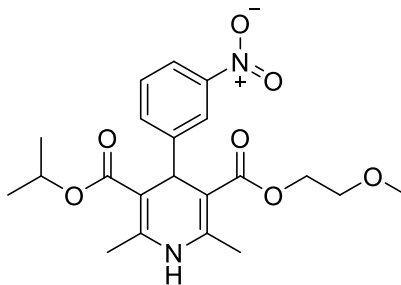
Etodolac
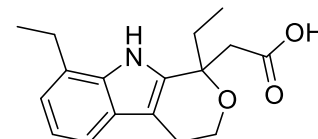
Table 1. Compound names and structure investigated on the Whelk-O (*S,S*)

14

Many of the separations showed that the efficiencies of the SPPs where higher than those of the FPP supports. In many cases, the 2.7 μm SPP packed column showed efficiencies that were approximately double the same separation on the 5 μm FPP packed column. In the constant mobile phase mode, efficiencies were calculated using the width at half-height using the Gaussian method (equation 1-4). The representative data seen in Figure 2. show substantial improvements in peak shape for the smaller core-shell particles. For the separations on the 2.7 μm SPP packed column, 1-acenaphthenone, oxazepam, hydrobenzoin, and Troger's base have efficiencies of 14400, 11200, 17500, and 10400 plates respectively. However, the same samples with the same mobile phase conditions using the 5 μm FPP packed column had efficiencies of 6800, 4500, 8300, and 6000 plates respectively. These results are analogous to the improvements for SPPs found for achiral stationary phases.

An advantage of this type of packing is that the retention times for the SPP column are always less than those on FPP counterparts. Additionally, the effective column volume is slightly reduced given that the column is partially occupied by nonporous cores [39]. Faster separations are considered more environmentally friendly because they will ultimately expend less resources like solvents or instrumental energy by analyzing the same number of samples in a shorter time period.

While the constant mobile phase mode showed considerable peak efficiency improvements in most of the compounds screened, some of the compounds seemingly violated the trend. Examples of these can be seen in Figure 3. Sulindac showed minimal improvement with an efficiency of 3000 plates on 2.7 μm SPP and 2700 plates on 5 μm

FPP. The case of chlormezanone is even more surprising as the 5 μm FPP column (4500 plates) outperformed the 2.7 μm SPP column (3200 plates). Anomalous cases such as these are what lead to more uncertain conclusions about this SPP CSP. A proposed explanation is that there is an increase in band broadening for SPP due to differences in bonded surface density. Gasparini estimates that there is approximately 20% more surface density of Whelk-O selector on SPP compared to fully porous particles of the same size [19]. This surface area difference slows mass transfer kinetics, contributing to more band broadening for SPP. While that no doubt contributes, this explanation does seem less significant given that even the anomalous cases spend less time in the column with SPPs than FPPs. Unfortunately, Regis did not provide the carbon loading of these columns. Several variables have not yet been properly accounted for making a fair comparison of SPP to FPP for enantiomeric separations challenging.

N₁= 14500

N1= 6800

Time/mins

N₁= 11100

N1= 4500

Time/mins

$N_1 = 17600$

N1= 8300

Time/mins

$N_1 = 10400$

$N_1 = 6100$

Time/mins
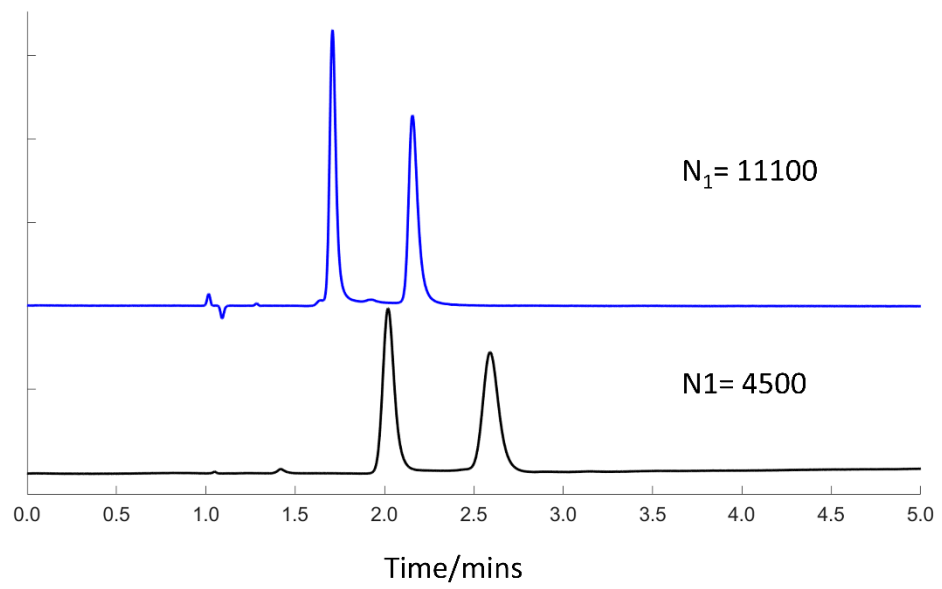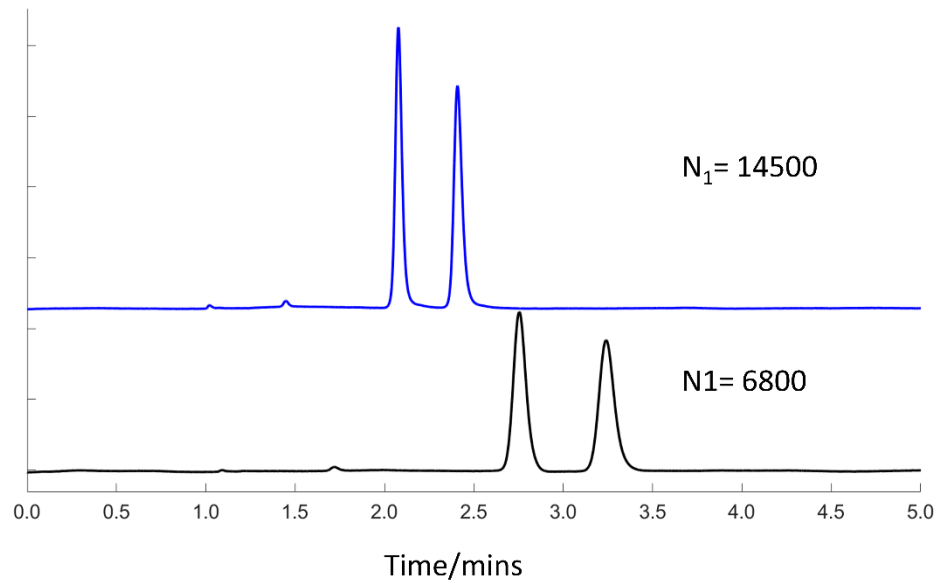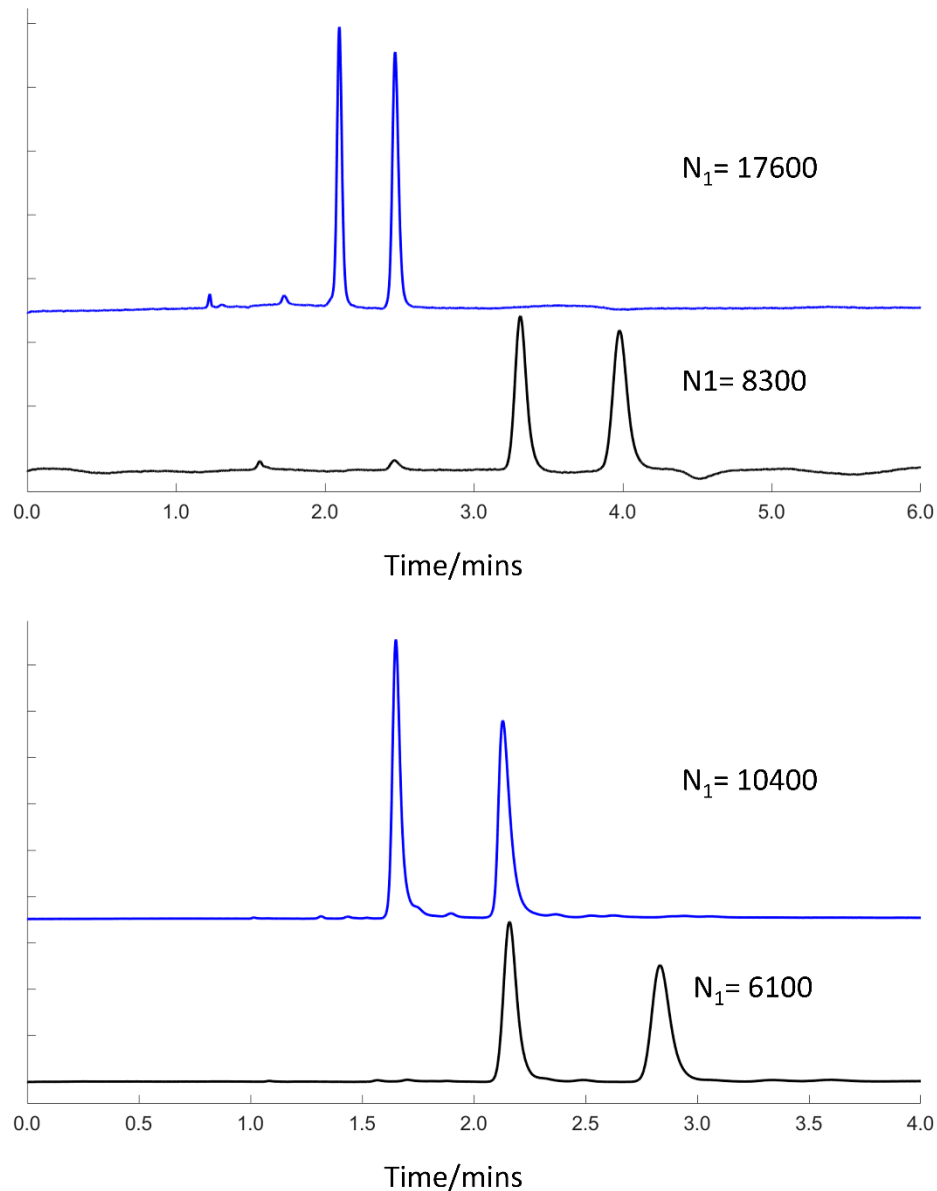
Figure 2. Constant mobile phase comparisons of enantiomeric separations on 2.7 μm SPP (blue chromatogram) and 5 μm FPP (black chromatogram). Chiral compounds shown in order of top to bottom are 1-acenaphthenone, oxazepam, Hydrobenzoin, and Troger's base. Time in minutes is shown on the x-axis. Whelk-O 1 (*S, S*) 10 cm x 0.46 cm i.d. 0.5 μL injection, 1.0 mL/min flow. 254 nm, 0.5 s response time. Oxazepam run on 40/60/0.3/0.2 ethanol/hexanes/TFA/TEA. Remained three ran with 20/80/0.3/0.2 ethanol/hexanes/AcOH/TEA.
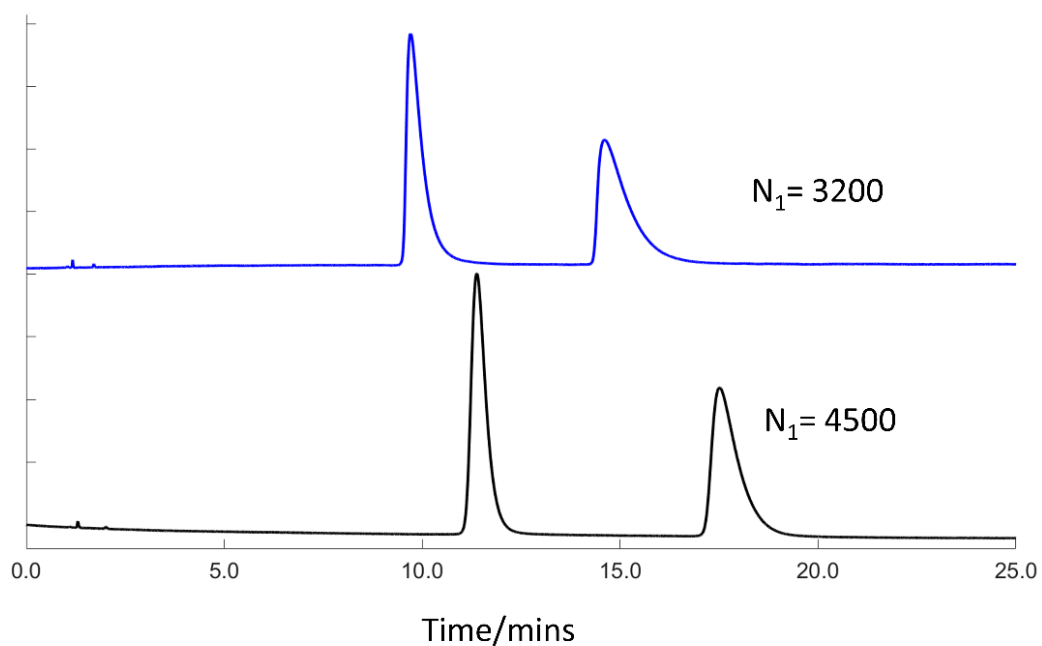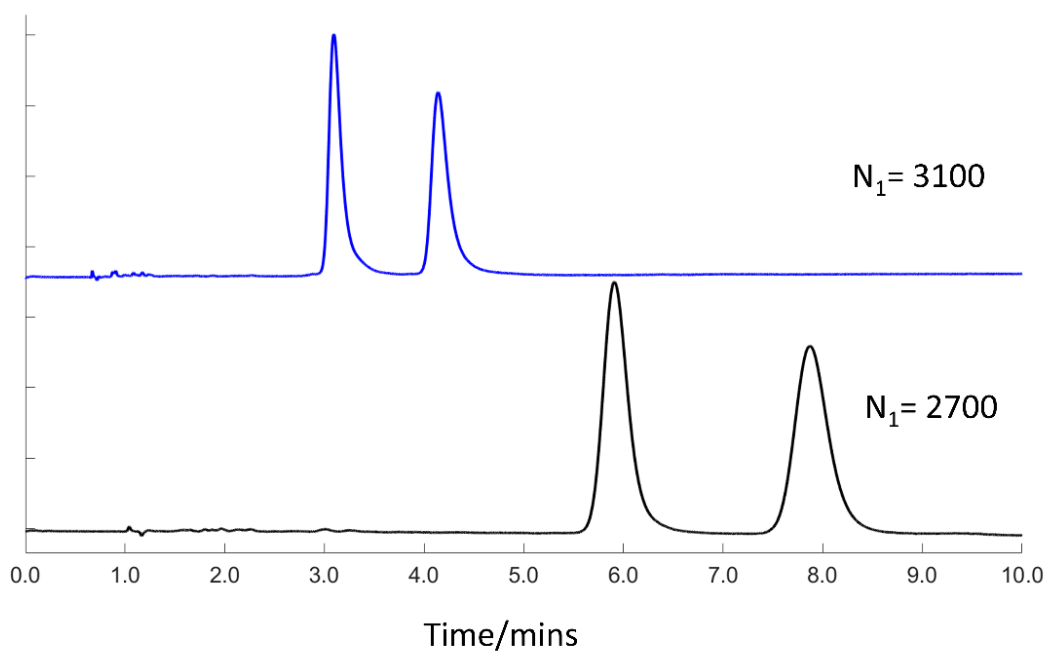
Figure 3. Constant mobile phase comparisons outliers of enantiomeric separations on 2.7 µm SPP (blue chromatogram) and 5 µm FPP (black chromatogram). Chiral compounds shown are sulindac on top and chlormezanone on bottom. Time in minutes is shown on the x-axis. Whelk-O 1 (*S, S*) 10 cm x 0.46 cm i.d. 0.5 µL injection, 1.0 mL/min flow. 0.5 s response time. Chlormezanone: 20/80 ethanol hexanes at 220 nm. Sulindac: 40/60/0.3/0.2 ethanol/hexanes/TFA/TEA at 254 nm.

#	Analyte	2.7 µm SPP				5 µm FPP			
		N_1	N_2	Resolution	Selectivity	N_1	N_2	Resolution	Selectivity
1	Troger's Base[a]	10400	8000	6.0	1.74	6100	5500	5.1	1.61
2	Carprofen[a]	2200	2600	3.1	1.44	3700	3500	6.1	1.67
3	5-methyl-5-phenylhydantoin[a]	13500	6600	7.4	1.85	5600	5000	5.9	1.70
4	Tetramisole[a]	1400	3000	8.6	2.44	2700	1300	3.8	1.53
5	Naproxen[a]	2300	3000	9.2	2.35	3900	4200	12.8	2.55
6	Coumarin[a]	1600	3600	3.7	1.39	3100	3700	6.2	1.59
7	Warfarin[a]	3600	5300	4.6	1.39	3700	3900	5.4	1.50
8	Trans-stilbene oxide[a]	17600	14500	11.2	2.33	8400	7500	10.00	2.37
9	Bendroflumethiazide[a]	3600	2400	2.7	1.27	3400	3000	3.0	1.27
10	Devrinol[a]	6600	2700	13.2	3.50	4600	3500	14.9	3.47
11	Ethotoin[a]	11300	6500	18.2	3.47	5900	4900	17.1	3.83
12	Trans-chlorostilbene oxide[a]	16300	13800	8.8	2.01	8000	7100	8.1	2.07
13	1-acenaphthenone[a]	14500	12800	4.3	1.31	6800	6500	3.3	1.29
14	Benzoin[a]	17400	14000	13.8	2.12	7500	6700	9.3	1.93
15	Bupivacaine[b]	14800	14700	3.7	1.27	6100	5700	2.8	1.25
16	Hydrobenzoin[b]	17600	15500	5.2	1.42	8300	7800	4.1	1.32
17	Chlormezanone[c]	3200	2000	4.9	1.58	4500	3600	6.6	1.60
18	Sulfinpyrazone[d]	600	700	2.7	1.63	1000	1000	3.2	1.55
19	Sulindac[d]	3100	3000	4.0	1.51	2700	2600	3.6	1.41
20	Nadifloxacin[e]	1500	900	3.5	1.64	2000	1610	4.3	1.59
21	Indapamide[d]	5800	3000	4.5	1.51	3100	2500	5.4	1.79
22	Tropicamide[d]	2700	1200	2.4	1.70	2800	1800	2.7	1.40
23	Oxazepam[d]	11100	8500	5.6	2.04	4500	3900	4.0	1.60
24	Ibuprofen[f]	11400	12200	3.3	1.27	7100	7000	3.3	1.17
25	Ketoprofen[f]	2300	3000	2.5	1.24	5300	5600	4.7	1.29
26	Flurbiprofen[f]	3500	3900	3.4	1.39	5500	5600	4.9	1.31
27	Nimodipine[g]	4100	3100	1.4	1.13	2800	2700	1.4	1.11
28	Etodolac[h]	9300	8300	2.41	1.12	5500	5400	8.81	1.12

Table 2. Chromatographic data for constant mobile phase mode on Whelk-O CSP bonded to 2.7 µm SPP and 5 µm FPP. Whelk-O 1 (*S, S*) 10 cm x 0.46 cm i.d. 0.1 µL injection, 1.0 mL/min flow. 254 nm, 0.5 s response time. Mobile phase a: 20/80/0.3/0.2 ethanol/hexanes/AcOH/TEA at 1 mL/min, b: 20/80/0.1/0.07 ethanol/hexanes/AcOH/TEA at 1 mL/min, c: 20/80 ethanol hexanes at 1 mL/min, 220 nm, d: 40/60/0.3/0.2 ethanol/hexanes/TFA/TEA at 1 mL/min. e: 40/60/0.3/0.2 ethanol/hexanes/TFA/TEA at 2 mL/min. f: 10/90/0.1/0.7 ethanol/hexanes/AcOH/TEA at 1 mL/min. g: 10/90/0.1/0.7 ethanol/hexanes/AcOH/TEA at 2 mL/min. h: 5/2/93/0.3/0.2 Isopropyl alcohol/methanol/hexanes/AcOH/TEA at 1 mL/min.

3.2. Additives in the mobile phase. Additives to the mobile phase are common in most forms of chromatography. Additives such as trifluoroacetic acid have demonstrated peak-sharpening effects [41]. Sub/supercritical fluid separations are particularly dependent on additives [42]. The value of additives translates to chiral chromatography. As previously mentioned, the slower kinetics of brush-like CSPs subjects the peaks to a higher degree of tailing [19]. Ideally, all other variables should be eliminated to determine if the advantages of SPP packings translates, as expected, from achiral separations to enantiomeric ones. Since performance evaluation methods are dependent on the shape of the peaks, practical means of mitigating peak distortions should be applied before comparing results. Here the use of additives in the mobile phase was tested to determine how they could affect peak shapes.

Acetic acid and triethylamine were added to the mobile phase to evaluate the effect on peak tailing. Peak tailing, T, was calculated according to equation 3-1 where $W_{0.05}$ is the total width of the peak at 5% of the maximum height, and $f_{0.05}$ is the distance of the leading edge to the peak mode at 5% of the maximum height. A tailing factor greater than 1 indicates tailing while a tailing factor less than 1 indicates fronting. In the case of Troger's base, the tailing factor without additives was found to be 2.0, but the peak was sharpened to have a tailing factor of 1.5 when 3% acidic acid and 2% triethylamine were added to the mobile phase. Consequently, the peak sharpening effect is positively reflected in the efficiency as the first peak efficiency is 10400 plates with the additives, but only 8000 plates without additives.

$$T = \frac{W_{0.05}}{2f_{0.05}}$$

0.3 AcOH 0.2 TEA
$N_1 = 10400$
$\alpha = 1.74$
$R_s = 5.97$

No Additives
$N_1 = 6700$
$\alpha = 1.36$
$R_s = 5.91$

Time/mins
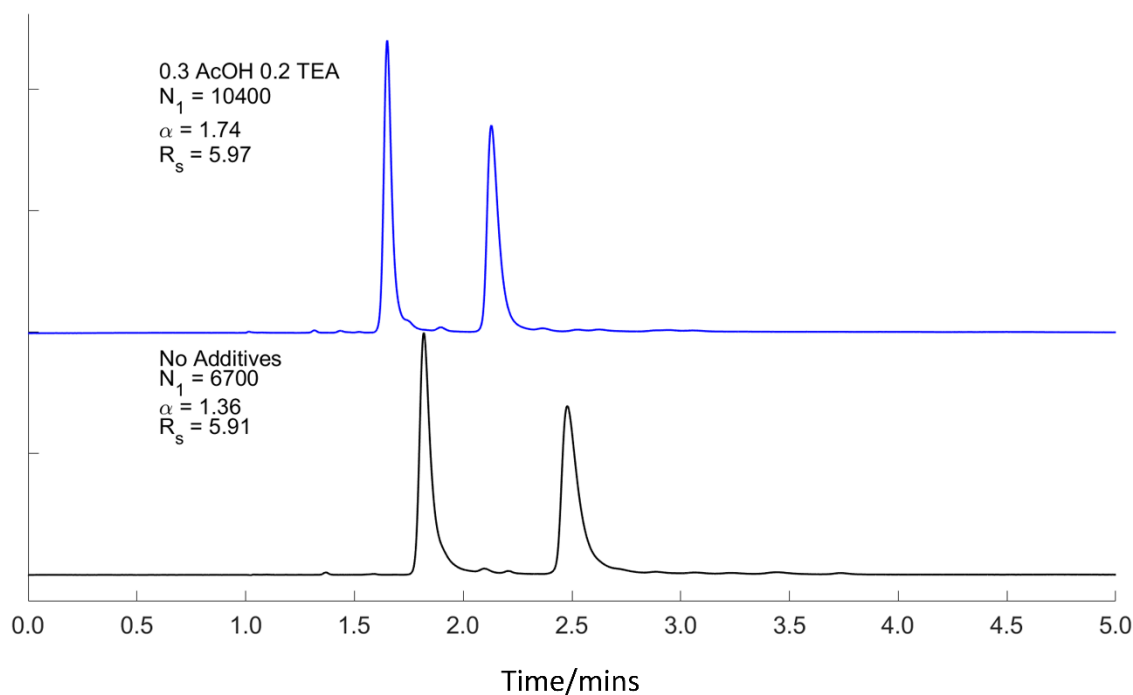
Figure 4. Chromatographic comparison of additives in the mobile phase. Troger's base is used as the analyte. Blue chromatogram shows a mobile phase with 0.3% acetic acid, and 0.2% triethyl amine. Black chromatogram shows the separation without additives. Whelk-O 1 (*S, S*) 10 cm x 0.46 cm i.d., 2.7 μm SPP, 0.5 μL injection, 1.0 mL/min flow. 0.5 s response time. 20/80 ethanol/hexanes.

The presence of acid or base additives in the mobile phase narrows the analyte band. The improvement is likely due to the additives acting in a mechanism similar to end-capping. Commercial CSPs are not end-capped exposing a greater amount of residual silanols which will cause a greater degree of band broadening [43]. The additives, like TEA, in the mobile phase helps alleviate this issue because the amine associates with the residual silanol. In the previously mentioned Troger's base example, the analyte is a base, so additives reduce the availability for the analyte to interact with residual silanols. Indeed, additives showed the best improvement for acidic and basic compounds as seen in figure 5. What is perhaps surprising is that neutral compounds also show peak shape improvement with the presence of additives. A degree of peak shape improvement can be seen in all tested cases.

Figure 5. Tailing factor in the presence of mobile phase additives subtracted from the tailing factor without additives. Compounds are clustered int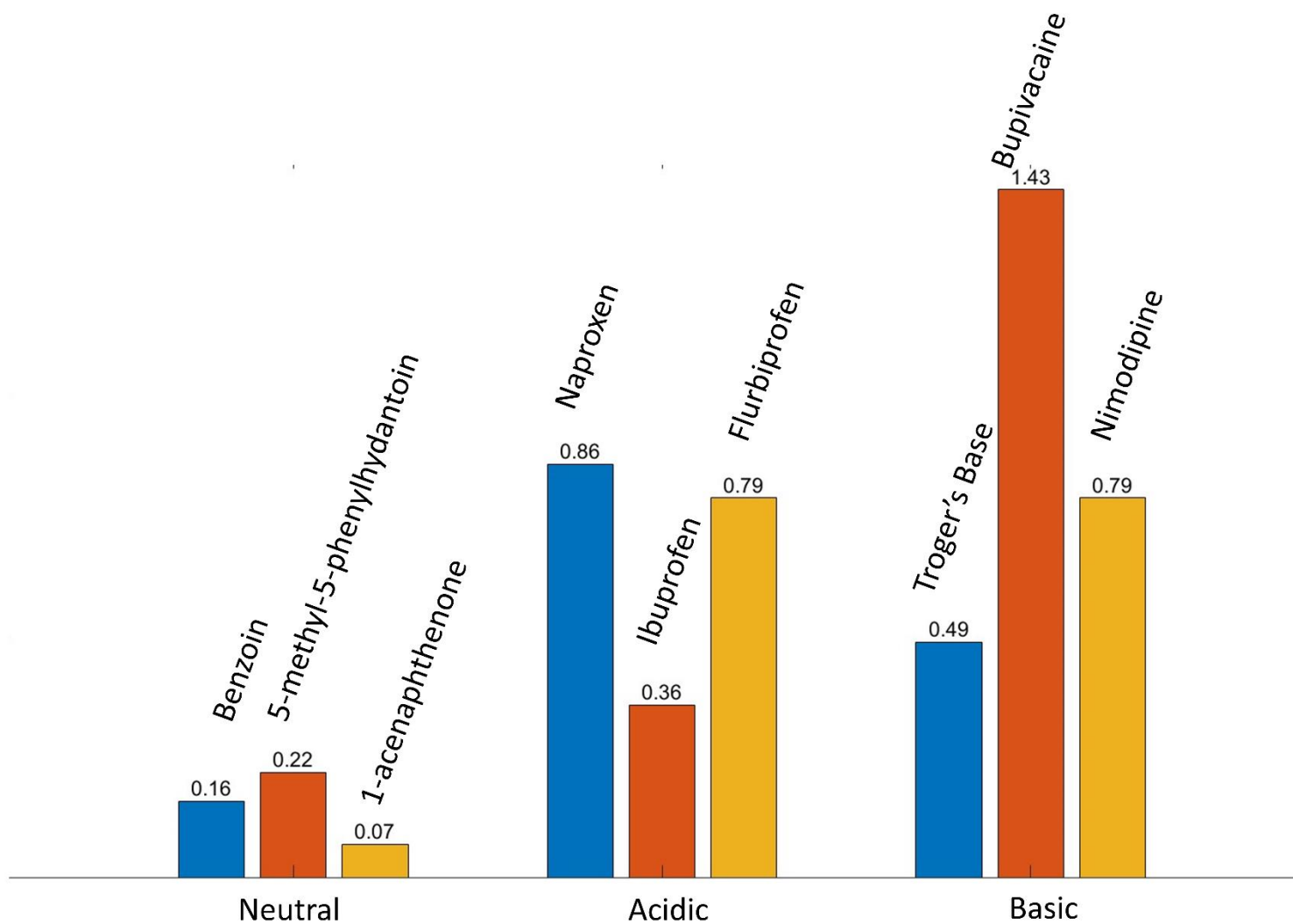o neutral, acidic, and basic compound groupings. Whelk-O 1 (*S, S*) 10 cm x 0.46 cm i.d., 2.7 µm SPP, 0.5 µL injection, 1.0 mL/min flow. 0.5 s response time. Specific mobile phases from table 2.

3.3. System peaks and solvent mismatch. While additives in the mobile phase have been proven to be valuable, continuous exposure of the analyte to acids or bases can result in decomposition of acid-base sensitive compounds. For this reason, additives are not necessarily used in sample solvents. Additionally, solubility issues may require that a different solvent be used in the sample than the mobile phase. This difference results in a degree of solvent mismatch with the mobile phase composition which can cause system peaks. A system peak is an isolated disturbance in the chromatogram as an artifact of the system rather than an analyte [40]. Commonly, the dead volume can be estimated by the system peak generated from the sample solvent briefly altering the refractive index of the mobile phase. As the sample solvent slug passes the column, it disturbs the local equilibrium of the additives between the two phases. A band of additives desorbs from the stationary phase and elutes shortly after the dead time. An additive void then passes through the column as it restores the local equilibrium [40]. These additive slugs and voids result in a system peak due to the lensing effect in the detector cell. These system peaks can sometimes cause interference with analyte peaks.

The issue of system peaks affecting peak shape can be seen in the separation of lorazepam (figure 6). Lorazepam standard is dissolved in methanol, but the mobile phase in the separation was a mixture of ethanol and hexanes. The system peak resulting from this solvent mismatch overlapped with the first enantiomer of the separation – making analysis of the peak performance impossible.

25
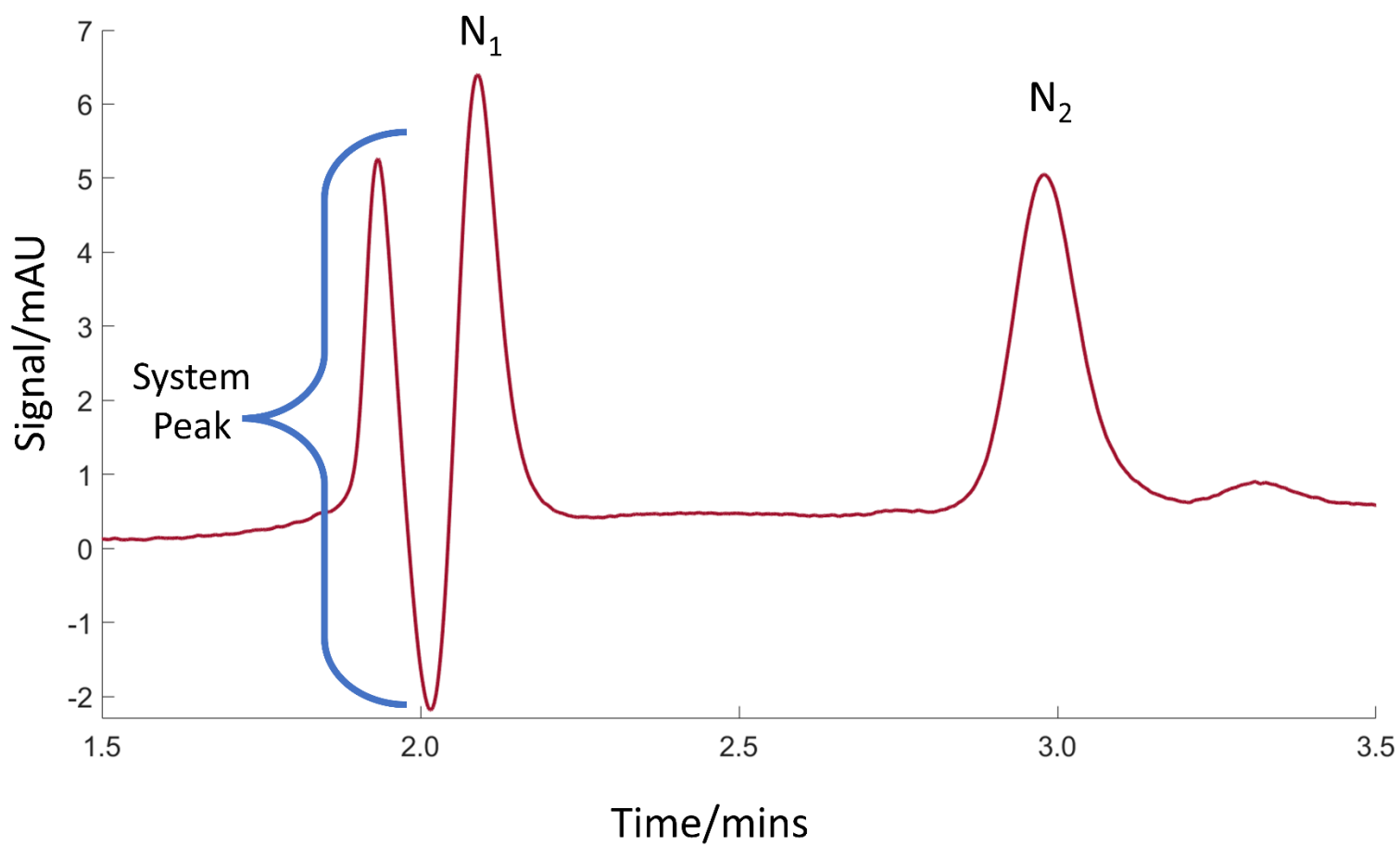
Figure 6. Separation of lorazepam on 2.7 μm SPP with a pronounced system peak. Whelk-O 1 (*S, S*) 10 cm x 0.46 cm i.d., 5 μm FPP, 0.5 μL injection, 1.0 mL/min flow. 0.5 s response time. 40/60/0.3/0.2 ethanol/hexanes/TFA/TEA.

The impact of sample solvent mismatch was tested by shooting solvent blanks (figure 7). A 20/80/0.3/0.2 ethanol/hexanes/AcOH/TEA mobile phase was prepared for this test. 0.5 µL injections of 10/90, 20/80, and 50/50 ethanol/hexanes without additives were studied at 254 nm. Additionally, blanks of pure ethanol, methanol, and 2-propanol were tested for system peaks on the same mobile phase. The results demonstrate that the system peak intensity was magnified as the sample solvent compositions were less like the mobile phase. The blank of pure methanol showed the strongest system peak signal. Interestingly, the 2-propanol blank injection resulted in several more system peaks compared to the other solvents. This phenomenon can be explained by the solvent traveling through the column in multiple paths because of mismatch with the eluent.

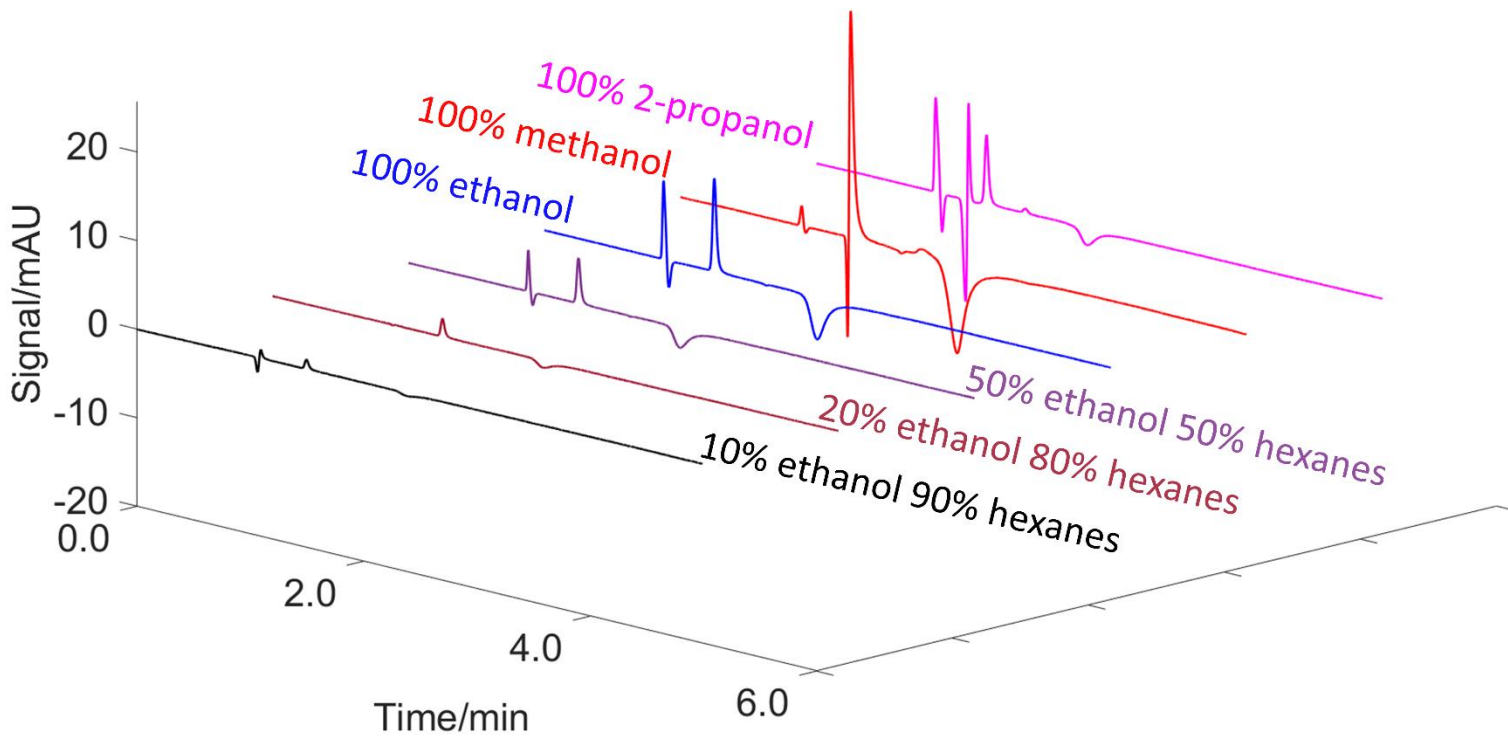Figure 7. Sample mismatch and system peaks of solvent blank 0.5 µL injections. Whelk-O 1 (*S, S*) 10 cm x 0.46 cm i.d., 2.7 µm SPP, 0.5 µL injection, 1.0 mL/min flow. 0.5 s response time.

In isolation, system peaks are of little consequence. However, if a system peak interferes with a sample peak like in the lorazepam example, then it will result in less accurate evaluations of a column's performance. To demonstrate this, *trans*-stilbene oxide was dissolved in the same solvents used in figure 7. The intensity of the system peaks continues to increase in the same pattern, but in the cases of methanol and propanol, there is significant interference (figure 8). Methanol results in a negative system peak that is detected at 2 mins and 15 seconds. That system peak destructively interferes with the second enantiomer which splits the peak, rendering analysis of it impossible. Conversely, the propanol resulted in a system peak that sharpens the slope of the first enantiomer. The result is that the efficiency of the artificially sharpened peak is estimated to be double when compared to other sample solvents. If the separation requires that the retention times remain unchanged, then methods to reduce system peaks should be employed.
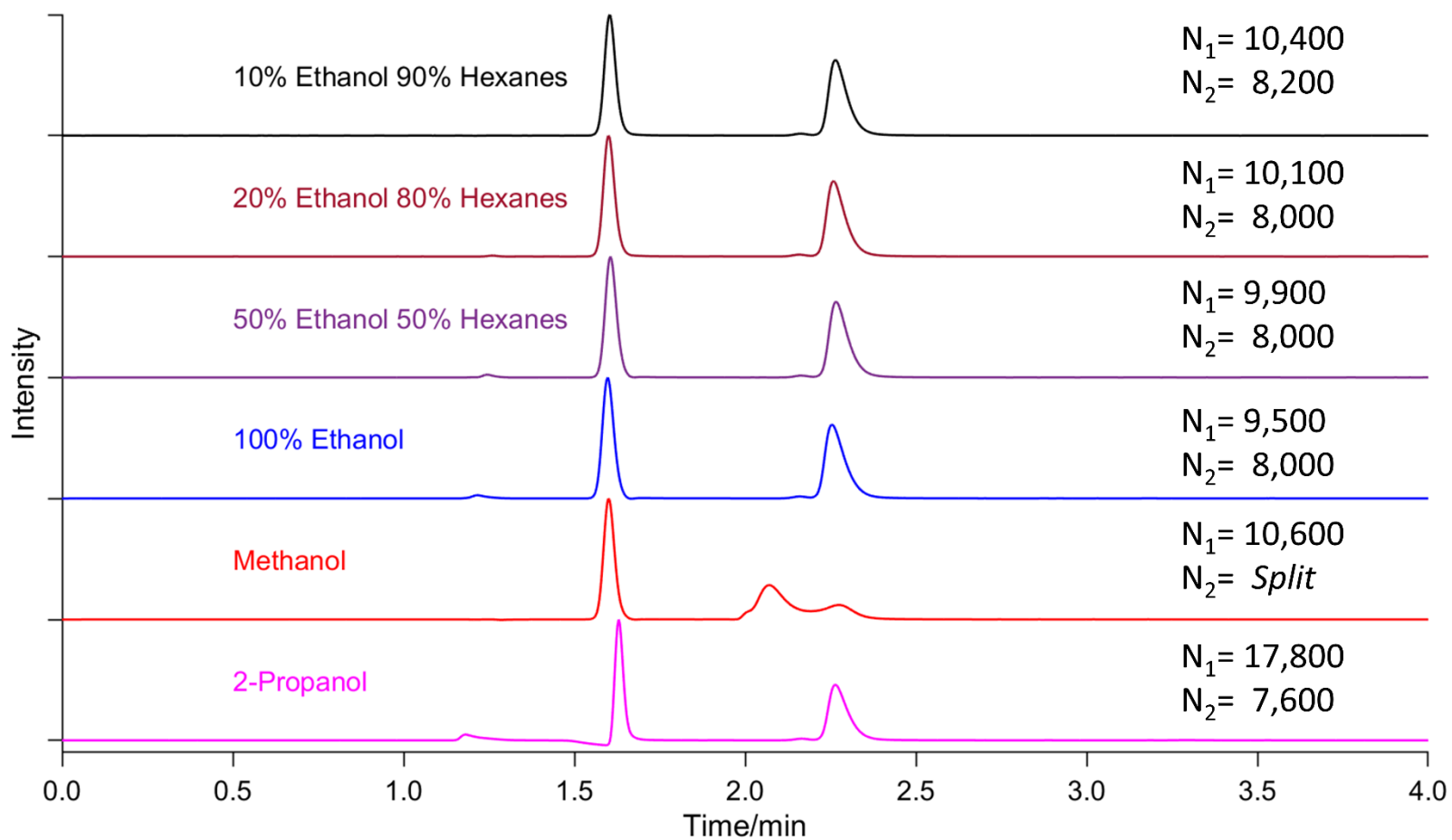
Figure 8. System peak interference in 0.5 μL injections of *trans*-stilbene oxide. Whelk-O 1 (*S, S*) 10 cm x 0.46 cm i.d., 2.7 μm SPP, 0.5 μL injection, 20/80/0.3/0.2 ethanol/hexanes/AcOH/TEA at 1.0 mL/min flow. 0.5 s response time.

To reduce the system peak interference, the tests were repeated using a smaller 0.1 µL injection volumes. Unsurprisingly, the pattern of system peak intensity was the same as in the larger injection volumes, although scaled to a proportionally smaller intensity. This can be seen in Figure 9. Since the mobile phase additives are UV transparent at 254 nm, the refractive index disturbance is not as pronounced when overlapping with a UV-absorbing compound. The same *trans*-stilbene oxide samples at smaller injection volumes alleviate the problematic system peak interference to a degree if not quite entirely (figure 10). For the sample dissolved in methanol, the second peak is noticeably weakened with the apparent efficiency to be reduced to 6700 plates, but the peak is no longer splitting. Similarly, the 2-propanol dissolved sample is much less impacted by the system peak interference. The first enantiomer appears to only have an increased plate efficiency of 400, compared to the previous injection that had a 7700 plate increase. This result suggests that the options for preventing system peak interference include picking a sample solvent that closely matches the mobile phase, as well as using smaller injection volumes.
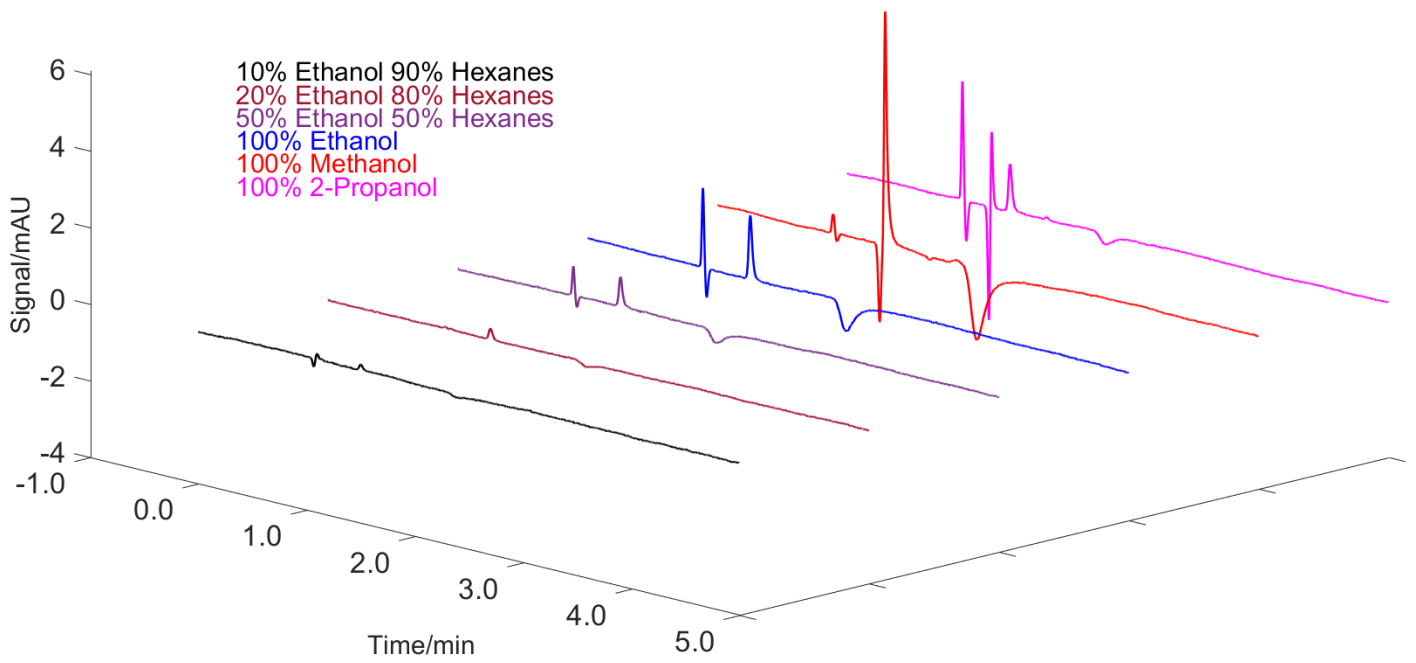
Figure 9. Sample mismatch and system peaks of solvent blank 0.1 µL injections. Whelk-O 1 (*S, S*) 10 cm x 0.46 cm i.d., 2.7 µm SPP, 0.1 µL injection, 1.0 mL/min flow. 0.5 s response time.

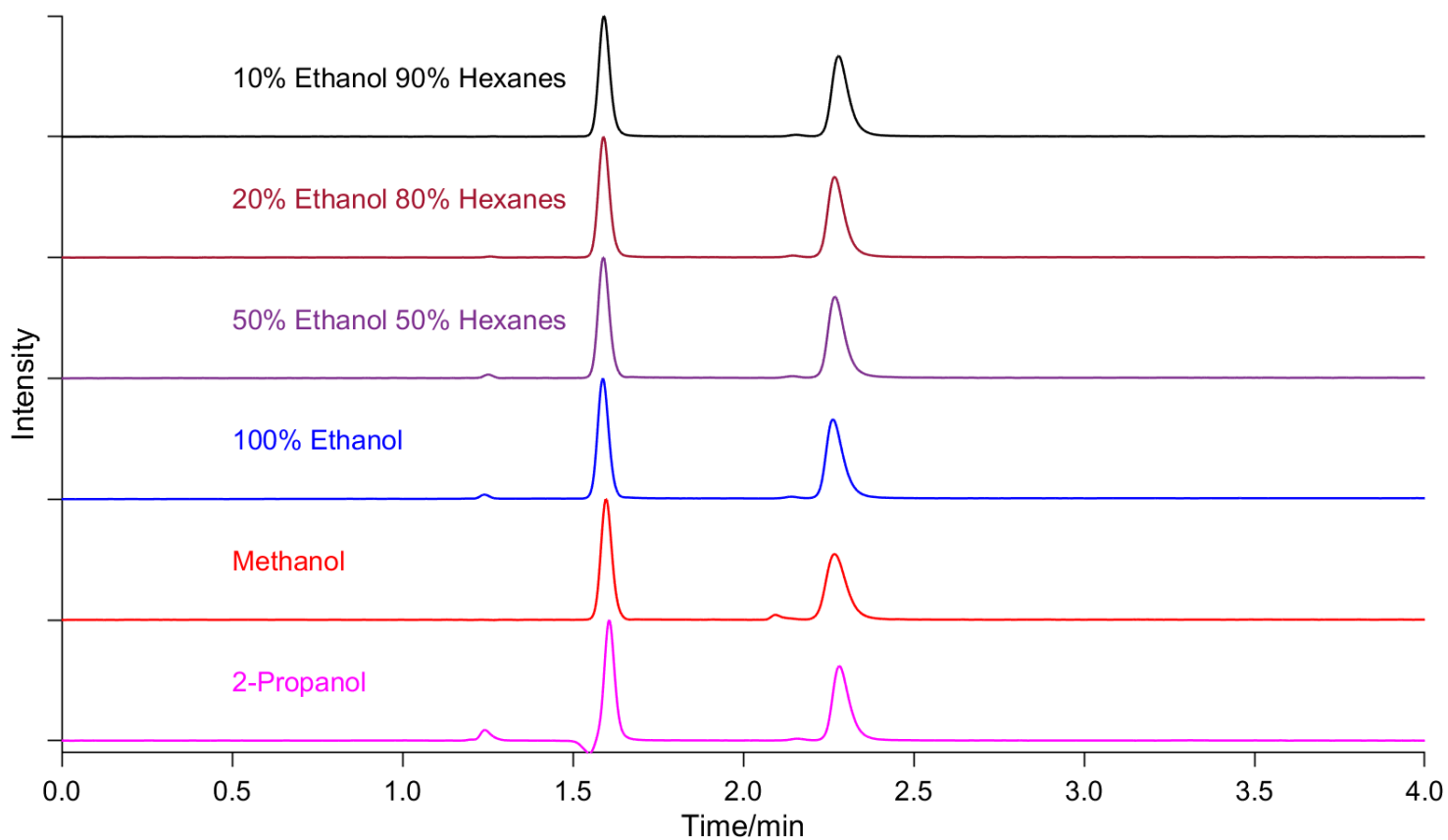Figure 10. System peak interference in 0.1 µL injections of *trans*-stilbene oxide. Whelk-O 1 (*S, S*) 10 cm x 0.46 cm i.d., 2.7 µm SPP, 0.5 µL injection, 20/80/0.3/0.2 ethanol/hexanes/AcOH/TEA at 1.0 mL/min flow. 0.5 s response time.

3.4 Peak model analysis. While the previously mentioned practical methods of

reducing peak shape distortions are valuable, normal phase enantiomeric separations

still exhibit a degree of peak asymmetry. When analyzing these peaks, it is often useful

to apply a peak-fitting model. When multiple peaks are not completely resolved,

mathematical techniques such as moment analysis can no longer be employed. The

benefit of peak-fitting models is that these peaks can be treated as though they are

isolated from neighboring peaks [29]. Additionally, a peak model will project a

completely smoothed baseline.

Previous results have all been reported using a Gaussian peak model which is

often a poor fit [44]. The accuracy of a model is reported using R^2 and the F-statistic.

Both values measure how much variation in the data is explained by the model

compared to how much of the data it does not explain. The R^2 is calculated according to

equation 3-2, where RSS is the residual sum of square differences between the observed

data values and the values predicted by the model, and the TSS is the sum of the square

difference between the values and the average value. A model more accurately

represents the data as the R^2 approaches 1. The F-statistic is found using equation 3-3,

where k is the number of predictors in the model and n is the total number of

observations. If the F-statistic is large, then the proposed model is a good fit for the data

[45].

$$R^2 = 1 - \frac{RSS}{TSS} \qquad\qquad 3\text{-}2$$

$$F = \frac{(\frac{RSS}{k})}{(\frac{RSS}{n-k-1})}$$

When Gaussian, GMG, and EMG models are fitted to enantiomeric separation done in the normal phase mode, the R^2 and F-statistic reveal that GMG and EMG much more accurately represent the data than the Gaussian model. The first enantiomer of chlormezanone separation was fitted with these models and shows an F-value of 94173 (R^2=0.998105) for EMG, 49926 (R^2=0.996431) for GMG, and only 3186 (R^2=0.934409) for Gaussian (figure 11). The performances of these peaks are able to be analyzed by the statistical moment of the models. In the chlormezanone example, the Gaussian model, GMG, and EMG reveal the efficiency to be 3404, 2479, and 1199 plates respectively. The reported differences for the same set of data are shockingly significant, revealing a general trend that the more sophisticated and accurate model produces peaks with lower efficiency.
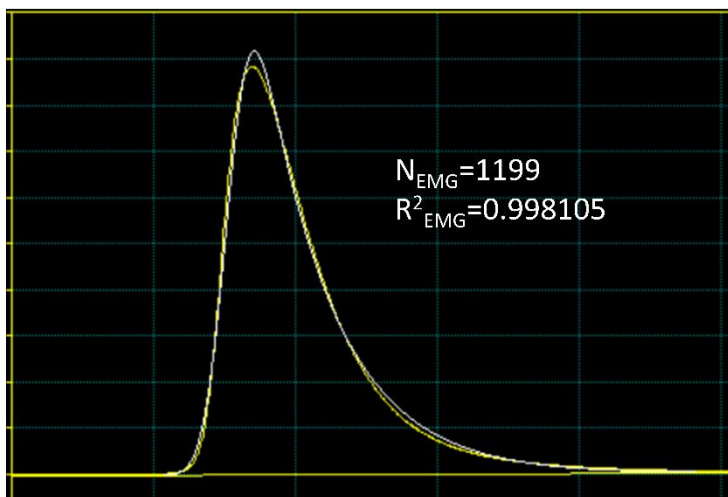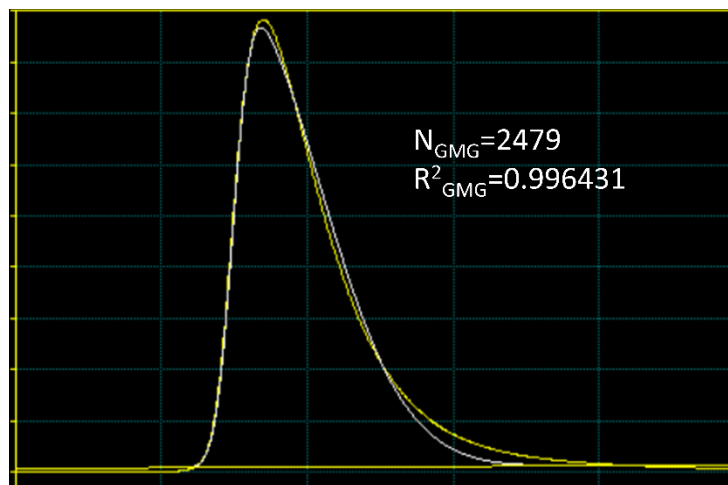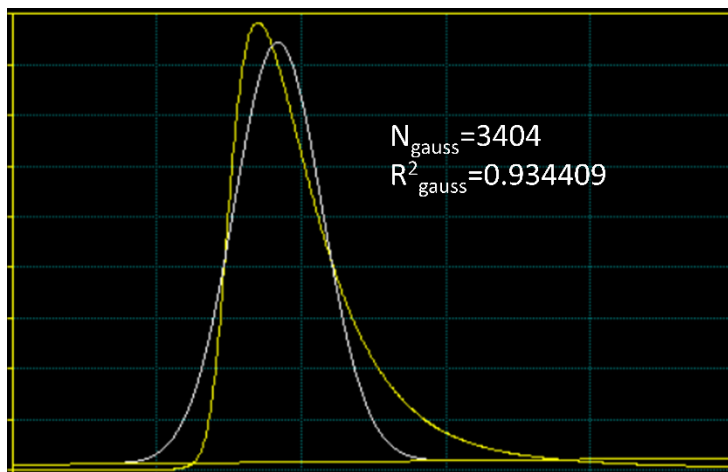
Figure 11. Peak fit models of chlormezanone first enantiomer. Model types are Gaussian on top, GMG in the middle, and EMG on bottom.

3.5 Particle packing comparison by peak fitting models. To better explain the differences of the SPP type column to the FPP packed columns, multiple models needed to be compared. Three drug compounds, ethotoin, ibuprofen, and indapamide, were selected for a detailed look using the constant retention mode (figure 12). The constant retention mode adjusts the strength of the mobile phase, so that the first enantiomer elutes at the same time in both column types. These separations aslo were repeated at a variety of flow rates to generate van Deemter plots.
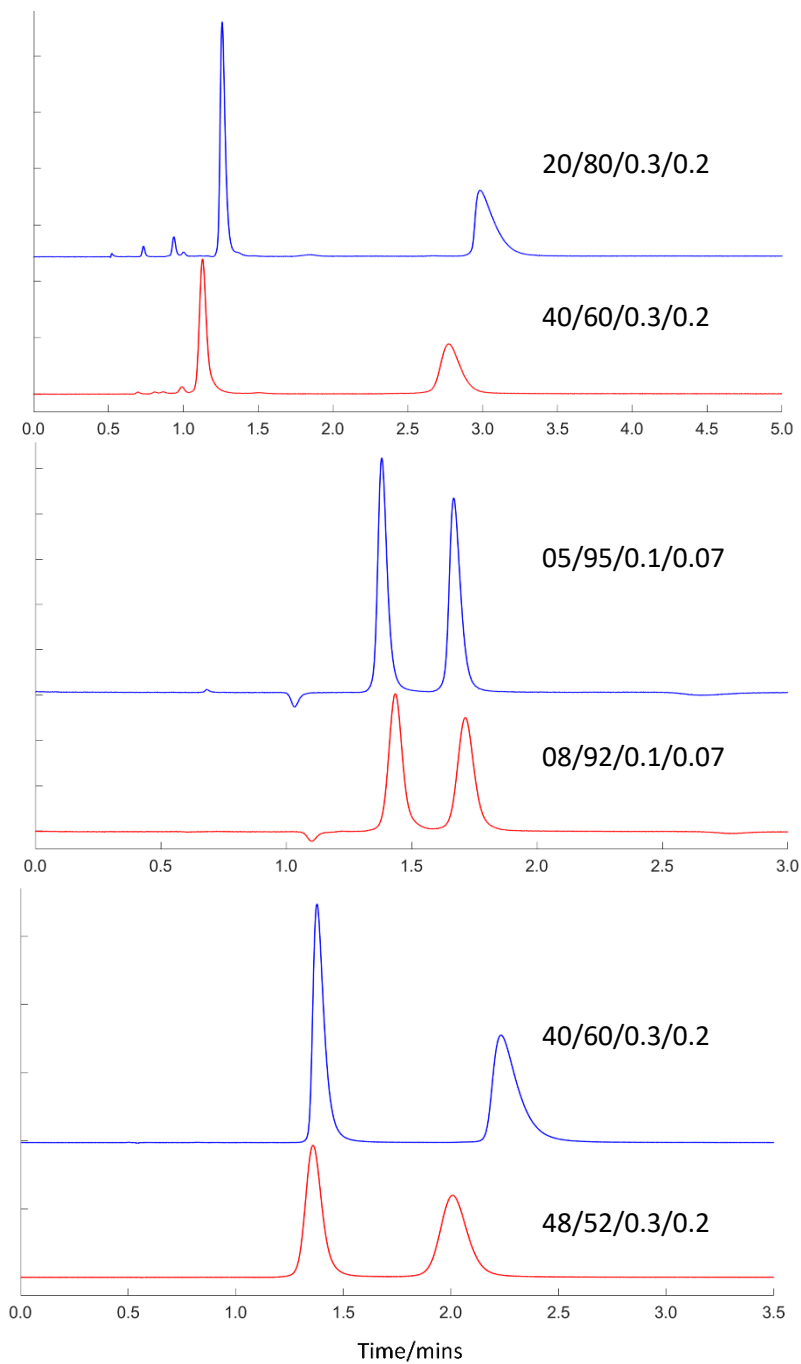
Figure 12. Ethotoin (top), ibuprofen (middle), and indapamide (bottom) comparison of 2.7 µm SPP (blue) to 5 µm FPP (red) in constant retention mode. Retention of the first enantiomer on the first column was within 95% similarity of the second column. Whelk-O 1 (*S, S*) 5 cm x 0.46 cm i.d., 2.7 µm SPP, 0.5 µL injection, 1 mL/min flow. 0.1 s response time. Ethotoin and ibuprofen run with ethanol/hexanes/AcOH/TEA. Indapamide run with ethanol/hexanes/TFA/TEA.

The van Deemter plot is a method of graphically representing intracolumn band broadening from the three most impactful sources [46]. Eddy diffusion accounts for multiple inequivalent pathways through the column and is unaffected by flow. Longitudinal diffusion occurs when analyte molecules diffuse in all directions of the column. Because longitudinal diffusion causes band broadening over time, higher flow rates reduce this as a contributing factor because the band spends less time in the column. Finally, the mass transfer term causes band broadening due to the velocity of the mobile phase being faster than the diffusion of molecules between the two phases. For liquid chromatography, mass transfer between flowing and stagnant mobile phases also contributes to band broadening. Higher flow rates provide less opportunity to reach equilibrium, so this term directly relates to the linear velocity. The minima in the van Deemter reveals required flow for optimized performance.

In all three cases, the minima in the van Deemter are lower for the 2.7 μm SPP column (figure 13). The H minima is more likely lower due to the smaller packing particle rather than the fact that one is superficially porous. It can also be seen that there are heating effects which are more pronounced on columns with smaller particle packing [47]. However, the slope of ascent is significantly depressed for columns with SPPs. These results suggest that SPP type packing is less affected by mass transfer compared to FPP. The reduced height can be found by dividing H by the particle size which allows for packing quality to be compared across differently sized particles in which a lower reduced plate height suggests a better packed column. The reduced plate height at the

van Deemter minima was found to be 2.67 on the 2.7 µm SPP and 2.22 on the 5 µm FPP.

The difference in packing quality is likely the best explanation for the unexpectedly poor

performance of some compounds on the SPP packed column. The real performance of

SPP can be even better demonstrated using kinetic plots.
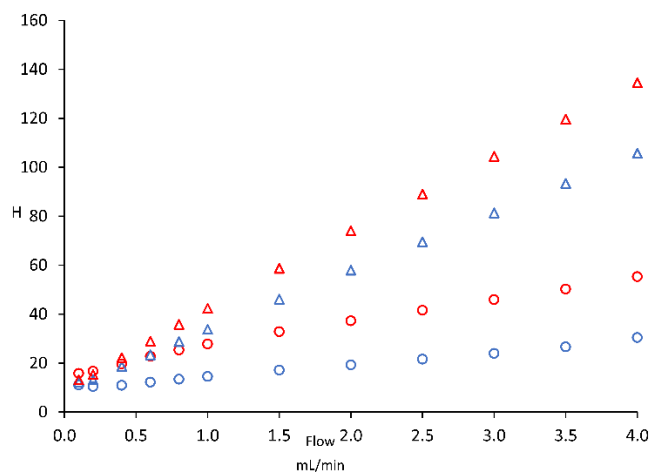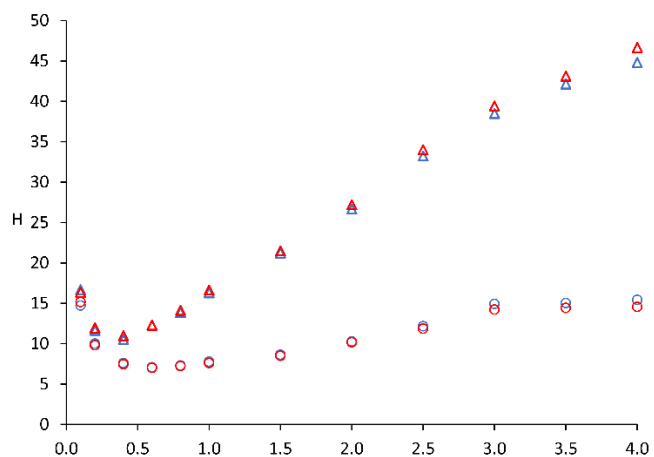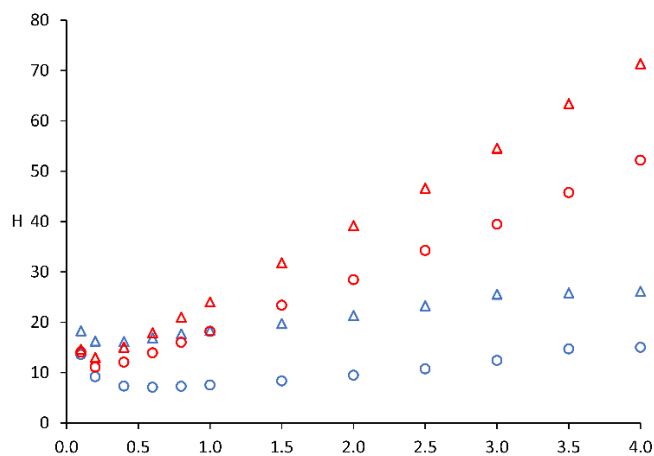
Figure 13. Van Deemter plots of ethotoin (top), ibuprofen (middle), and indapamide (bottom). The first and second enantiomers are shown in blue and red respectively. 2.7 μm SPP depicted as circles and 5 μm FPP as triangles. Whelk-O 1 (*S, S*) 5 cm x 0.46 cm i.d., 2.7 μm SPP, 0.5 μL injection. 0.1 s response time, using constant retention mode. Ethotoin and ibuprofen run with ethanol/hexanes/AcOH/TEA. Indapamide run with ethanol/hexanes/TFA/TEA.

Kinetic plots are graphical methods for studying mass transfer kinetics within chromatographic columns. The efficiency of the separation is plotted on the x-axis and the dead time is plotted on the y-axis [48]. This method of scaling magnifies the measurements that are concentrated around the minima on the van Deemter. Kinetic plots detail what dead time ranges would be required for a desired efficiency. Kinetic plots of ibuprofen on the 2.7 μm SPP column and 5 μm FPP column (figure 14) show the stark kinetic advantage of superficially porous packing. Based on these results as well as van Deemter plots, it is clear that the kinetics of superficially porous particles are superior to fully porous particles. The claim that chiral selector density negatively affecting mass transfer kinetics is a less valid explanation for underperforming cases. Conversely, poor column packing is supported by the reduced plate height calculations.
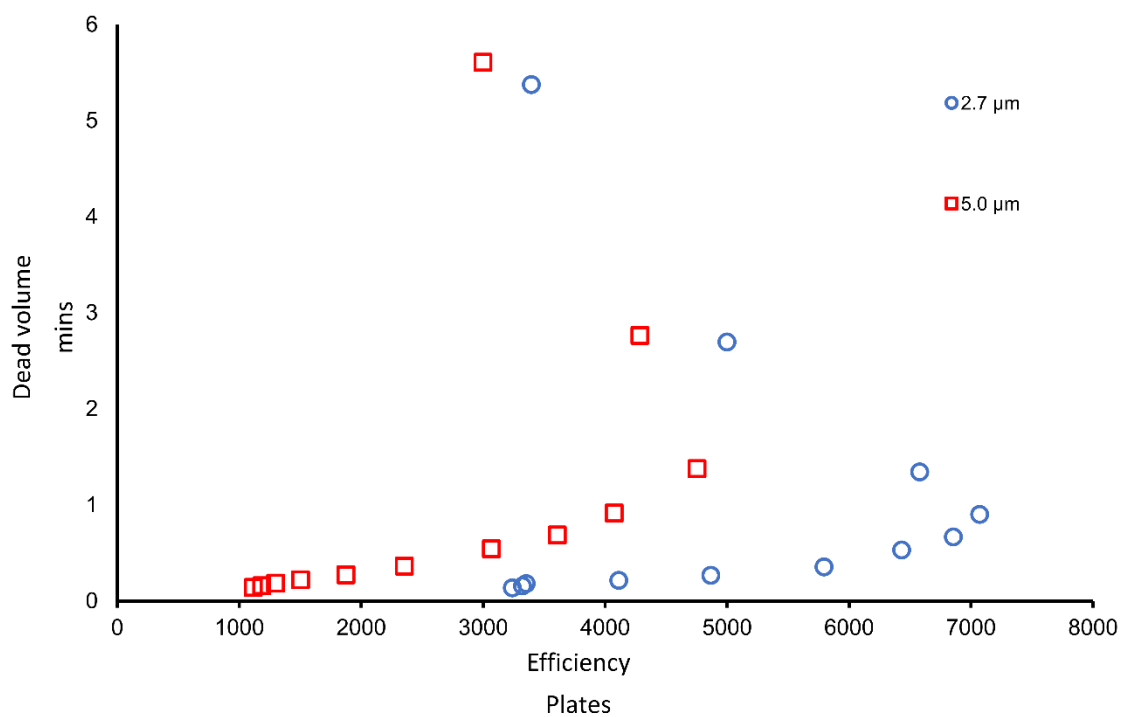
Figure 14. Kinetic plot of the first ibuprofen enantiomer. Data collected using 2.7 μm SPP column is represented with black circles, and 5 μm FPP is represented with red squares. Whelk-O 1 (*S, S*) 5 cm x 0.46 cm i.d., 2.7 μm SPP, 0.5 μL injection. 0.1 s response time, using constant retention mode. 05/95/0.1/0.07 and 08/92/0.1/0.07 ethanol/hexanes/AcOH/TEA for SPP and FPP respectively.

Lastly, the previously mentioned peak models were applied to the kinetic plot data sets (figures 15-20). A model free moment analysis derived using equation 1-5 was also graphed and served as the most accurate reference point of the other modeling methods. These kinetic plots continue to show the same efficiency trend with Gaussian models having the highest and EMG having the lowest. In most cases, kinetic plots of the EMG model most closely resembled the model free moment analysis, which is consistent with the R^2 or F-statistic evaluations. The one exception to this is the second enantiomer of ethotoin (figure 15) which shows GMG as slightly better at matching the model free moment analysis results. This result is not surprising, as GMG was designed to better account for intracolumn band broadening. The second enantiomer is retained longer, so intracolumn band broadening becomes more significant than extra-column effects. What is perhaps more surprising is that EMG was most accurate for the second enantiomer of all other compounds including the same ethotoin sample on the 5 μm FPP column. If models are to be applied when comparing results, it is necessary to fit the most accurate model on case-by-case basis in order to draw a fair conclusion.

Figure 15. Kinetic plot of the first (top) and second (bottom) enantiomer of ethotoin by different peak fitting models. Whelk-O 1 (*S, S*) 5 cm x 0.46 cm i.d., 2.7 μm SPP, 0.5 μL injection. 0.1 s response time. 20/80/0.3/0.2 ethanol/hexanes/AcOH/TEA.
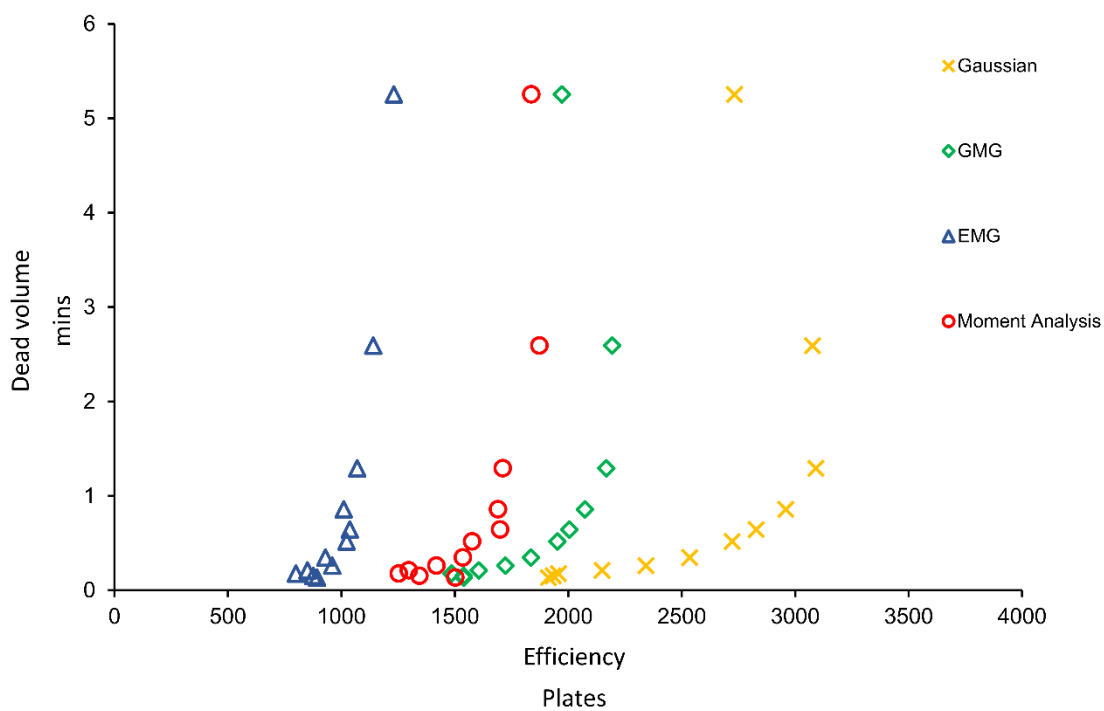
Figure 16. Kinetic plot of the first (top) and second (bottom) enantiomer of ethotoin by different peak fitting models. Whelk-O 1 (*S, S*) 5 cm x 0.46 cm i.d., 5 μm FPP, 0.5 μL injection. 0.1 s response time. 40/60/0.3/0.2 ethanol/hexanes/AcOH/TEA.

Figure 17. Kinetic plot of the first (top) and second (bottom) enantiomer of ibuprofen by different peak fitting models. Whelk-O 1 (*S, S*) 5 cm x 0.46 cm i.d., 2.7 μm SPP, 0.5 μL injection. 0.1 s response time. 05/95/0.1/0.07 ethanol/hexanes/AcOH/TEA.

Figure 18. Kinetic plot of the first (top) and second (bottom) enantiomer of ibuprofen by different peak fitting models. Whelk-O 1 (*S, S*) 5 cm x 0.46 cm i.d., 5 μm FPP, 0.5 μL injection. 0.1 s response time. 08/92/0.1/0.07 ethanol/hexanes/AcOH/TEA.
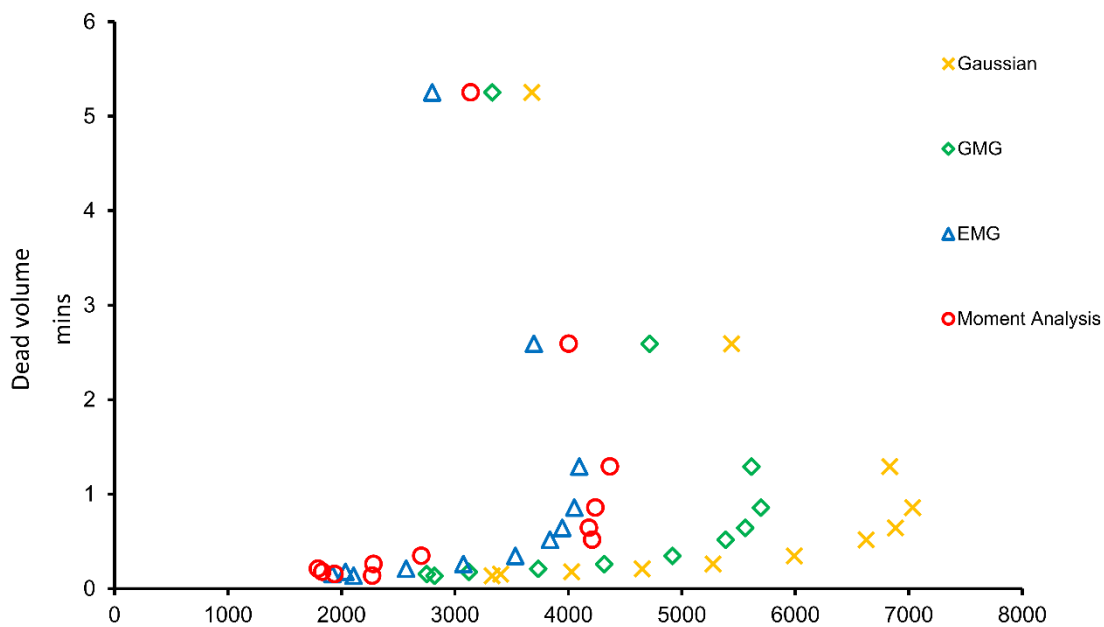
Figure 19. Kinetic plot of the first (top) and second (bottom) enantiomer of indapamide by different peak fitting models. Whelk-O 1 (*S, S*) 5 cm x 0.46 cm i.d., 2.7 µm SPP, 0.5 µL injection. 0.1 s response time. 40/60/0.3/0.2 ethanol/hexanes/TFA/TEA.
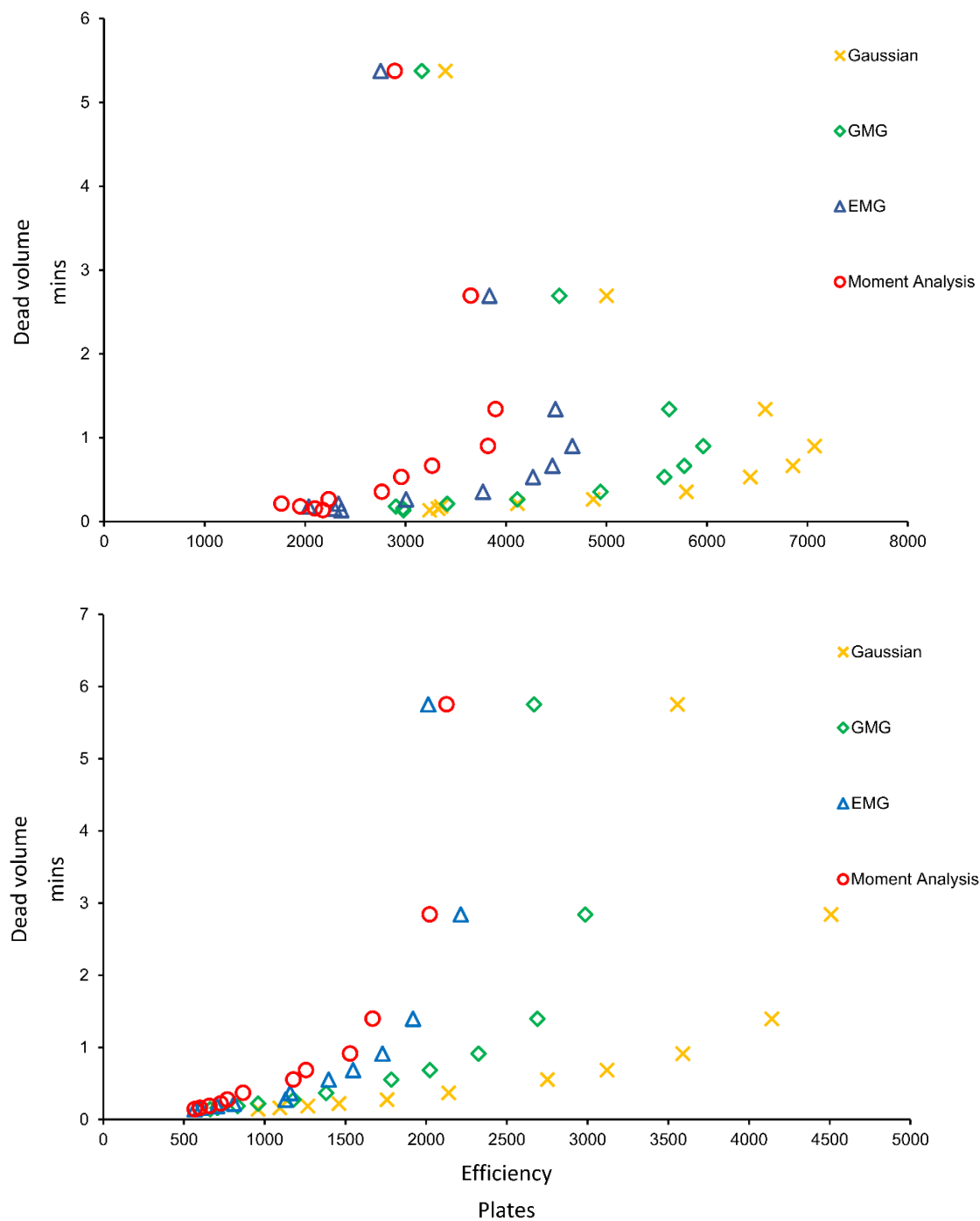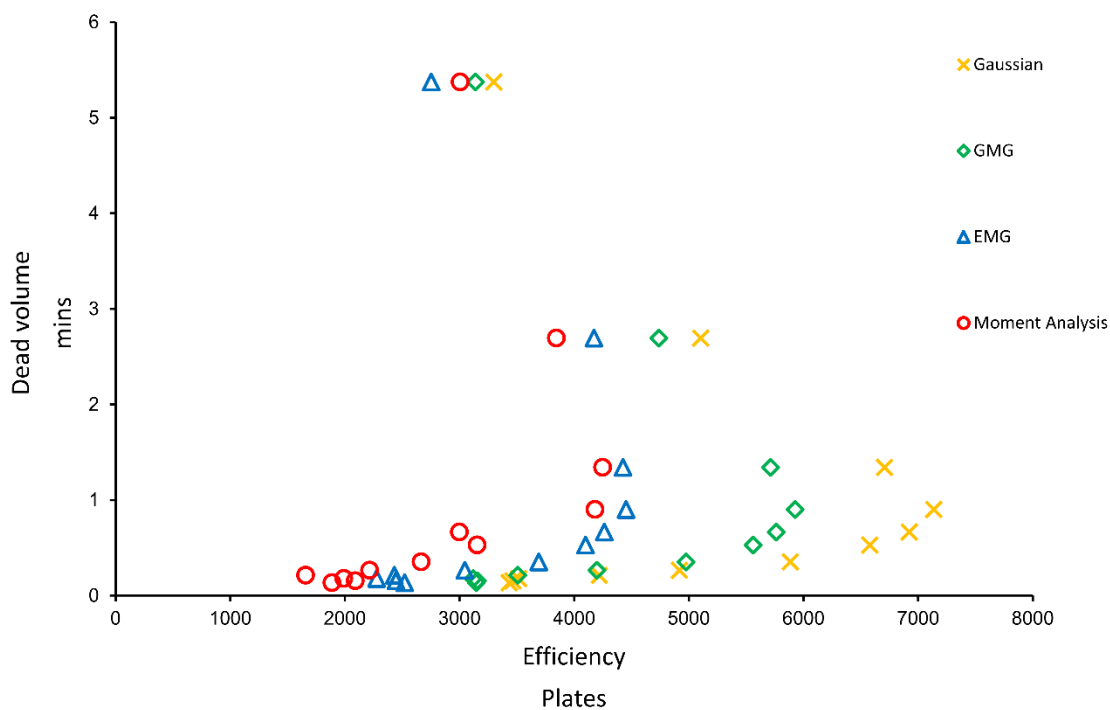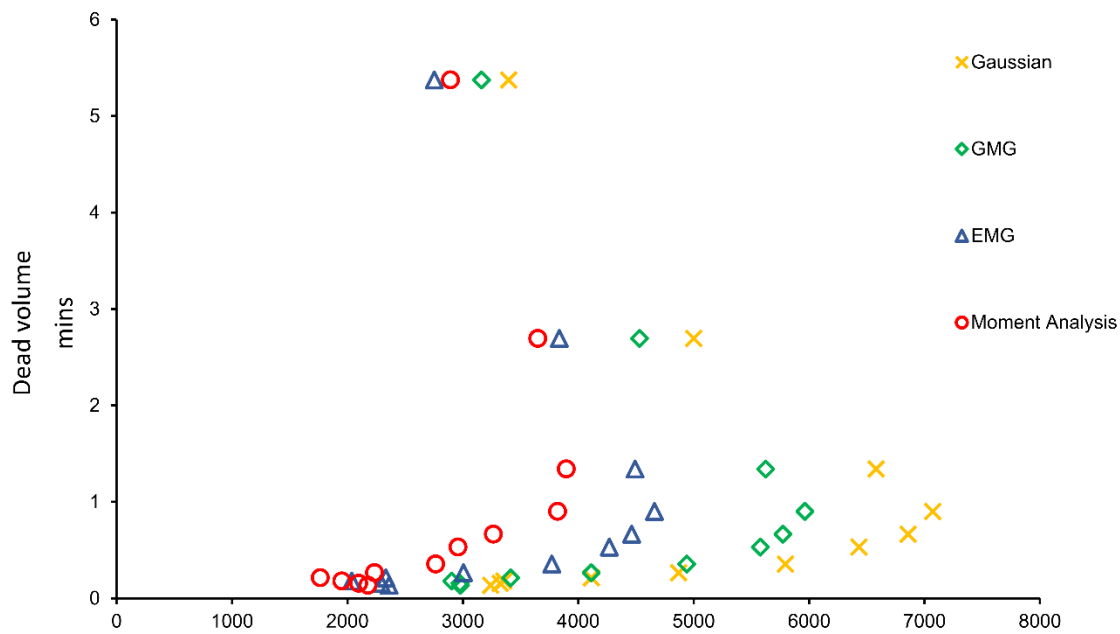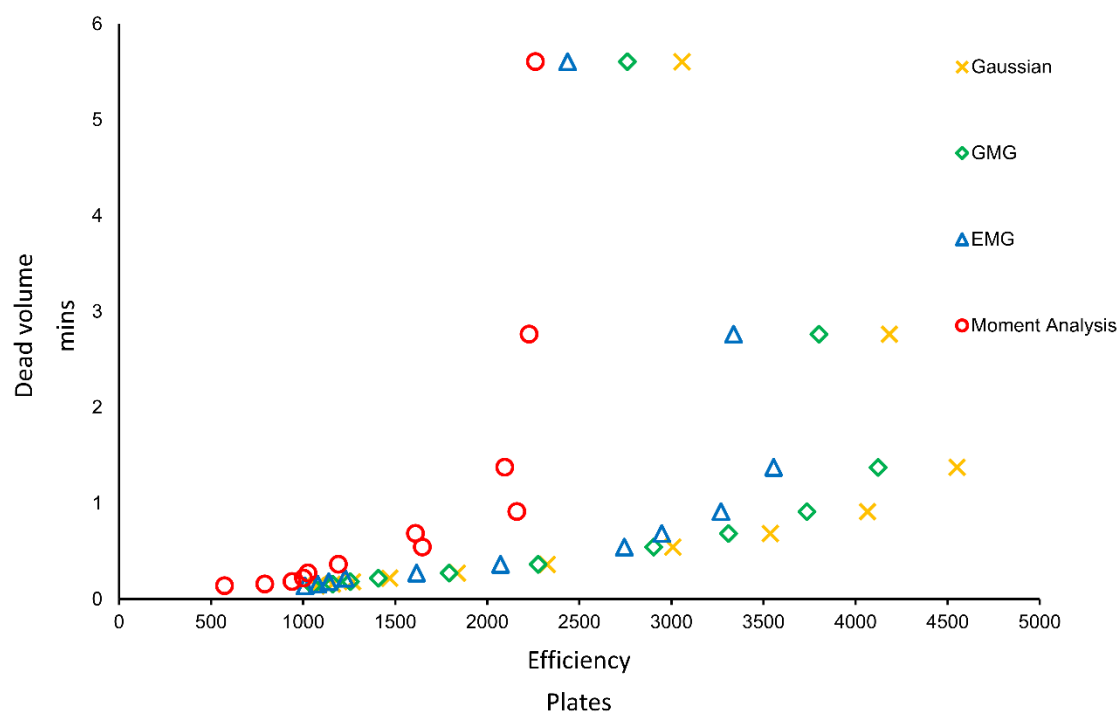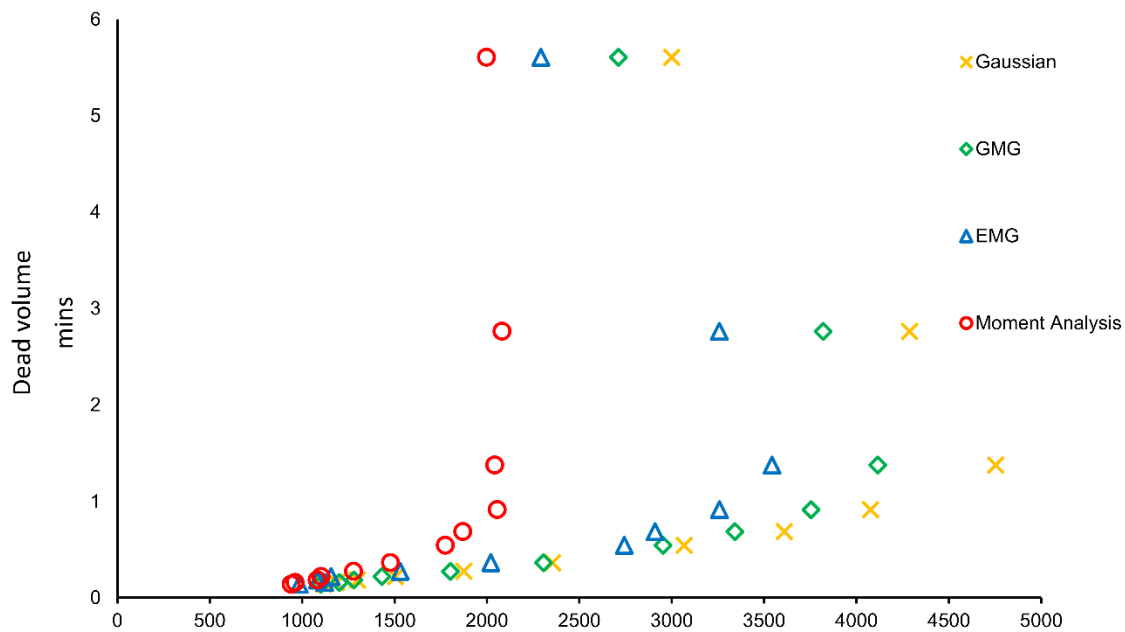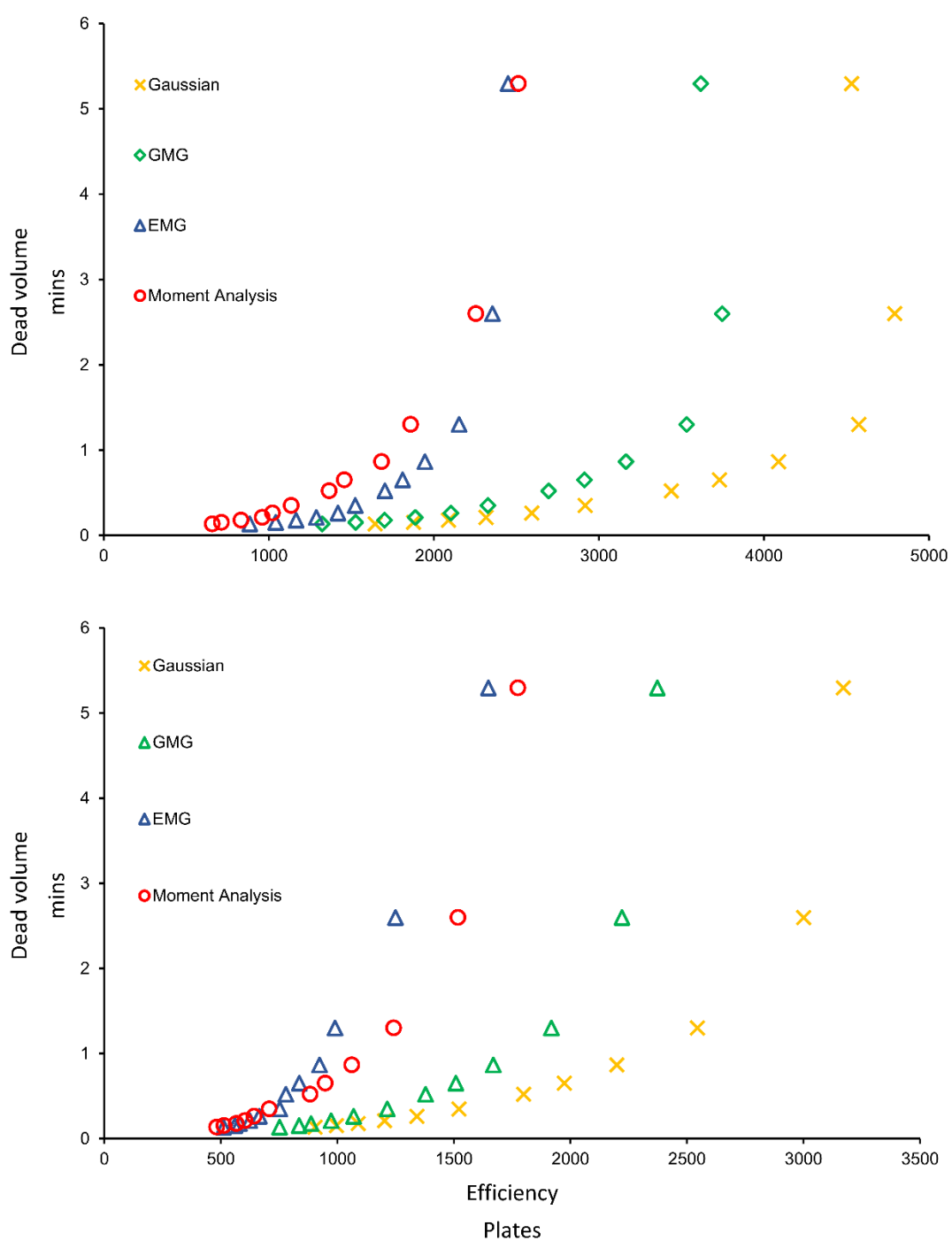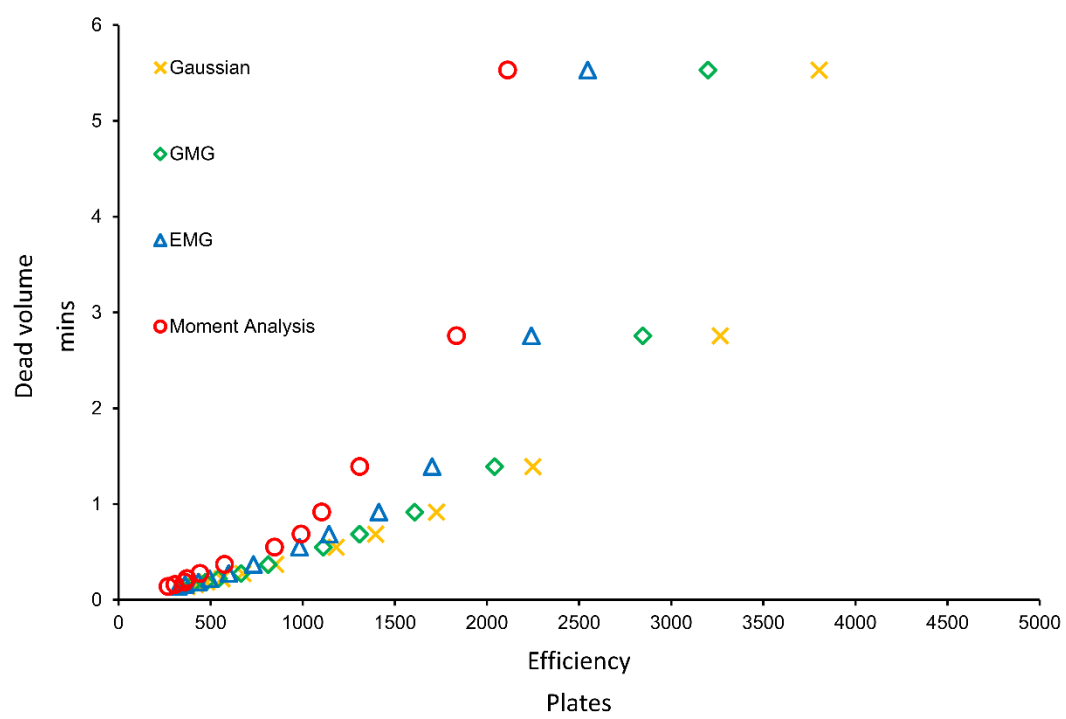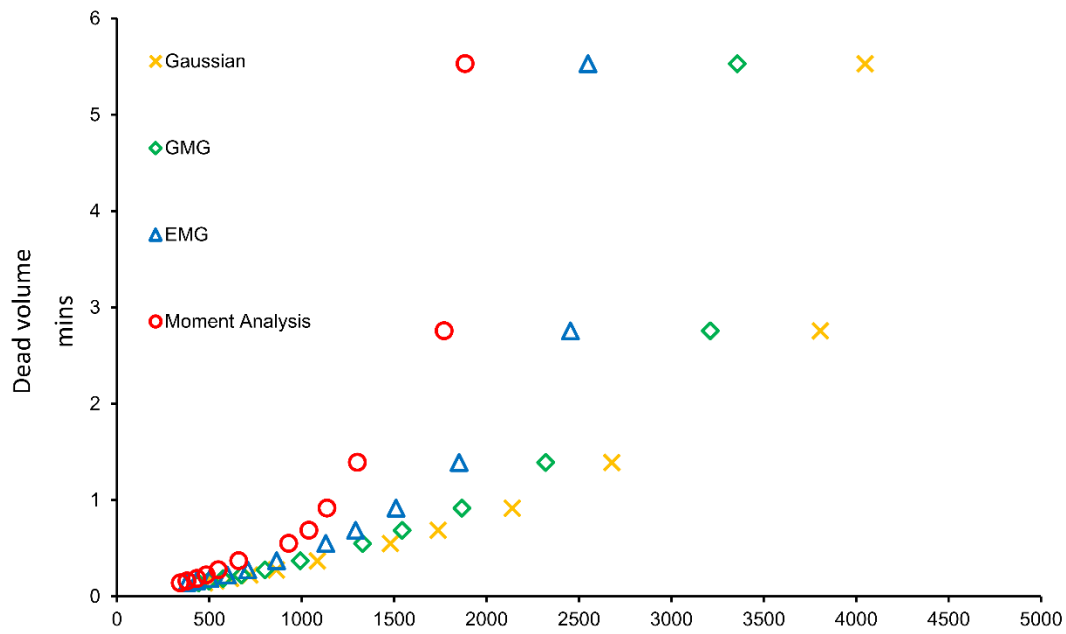
Figure 20. Kinetic plot of the first (top) and second (bottom) enantiomer of indapamide by different peak fitting models. Whelk-O 1 (*S, S*) 5 cm x 0.46 cm i.d., 5 μm FPP, 0.5 μL injection. 0.1 s response time. 48/52/0.3/0.2 ethanol/hexanes/TFA/TEA.

4. *Conclusions*

The experimental study of peak shape distortions demonstrates that the value of core shell type particles translates to normal phase chiral chromatographic separations. Some chiral separations do not perform as well on SPP as FPP which is consistent with the literature, but the reason for this is likely due to the quality of packing rather than the density of the chiral selector. Peak shape asymmetry was better addressed to draw a more conclusive result. Additives to the mobile phase and minimizing system peak interference are practical methods for reducing peak shape distortions. The remaining peak asymmetry is accounted for by the application of more sophisticated peak fitting models than Gaussian distribution. For future work, the 2.7 μm SPP column should be repacked to achieve a reduced plate height more comparable with FPP. The value of SPP particles in enantiomeric separations are likely to be affirmed if packing quality significantly improves the cases of unexpectedly inefficient separations. Additionally, other models can be tested. Hybrid models like EMG-GMG or Haaroff-Van der Linde (HVL) will likely fit these peak shapes better to make comparisons even more fair.

References

[1]   H Brooks, W., C Guida, W., G Daniel, K., The significance of chirality in drug design and development. Curr. Top. Med. Chem. 2011, 11, 760-770

[2]   Moss, G. P., Basic terminology of stereochemistry (IUPAC Recommendations 1996). Pure Appl. Chem. 1996, 68, 2193-2222

[3]   Wahab, M. F., Weatherly, C. A., Patil, R. A., Armstrong, D. W., in: Chiral Analysis. Elsevier, 2018, pp. 507-564.

[4]   Vargesson, N., Thalidomide-induced teratogenesis: History and mechanisms. Birth Defects Res. C. Embryo Today Rev. 2015, 105, 140-156

[5]   Tokunaga, E., Yamamoto, T., Ito, E., Shibata, N., Understanding the thalidomide chirality in biological processes by the self-disproportionation of enantiomers. Scientific reports. 2018, 8, 17131

[6]   Tomaszewski, J., Rumore, M. M., Stereoisomeric drugs: FDA's policy statement and the impact on drug development. Drug Dev. Ind. Pharm. 1994, 20, 119-139

[7]   Armstrong, D. W., DeMond, W., Cyclodextrin bonded phases for the liquid chromatographic separation of optical, geometrical, and structural isomers. J. Chromatogr. Sci. 1984, 22, 411-415

[8]   Chen, X., Yamamoto, C., Okamoto, Y., Polysaccharide derivatives as useful chiral stationary phases in high-performance liquid chromatography. Pure Appl. Chem. 2007, 79, 1561-1573

[9]   Lämmerhofer, M., Chiral recognition by enantioselective liquid chromatography: mechanisms and modern chiral stationary phases. Journal of Chromatography A. 2010, 1217, 814-856

[10]   Boehm, R. E., Martire, D. E., Armstrong, D. W., Theoretical considerations concerning the separation of enantiomeric solutes by liquid chromatography. Anal. Chem. 1988, 60, 522-528

[11]   Patel, D. C., Breitbach, Z. S., Wahab, M. F., Barhate, C. L., Armstrong, D. W., Gone in seconds: praxis, performance, and peculiarities of ultrafast chiral liquid chromatography with superficially porous particles. Anal. Chem. 2015, 87, 9137-9148

[12]   Scriba, G. K., Chiral recognition in separation science–an update. Journal of Chromatography A. 2016, 1467, 56-78

[13]   Lipkowitz, K. B., Theoretical studies of brush-type chiral stationary phases. Journal of Chromatography A. 1994, 666, 493-503

[14]   Kotoni, D., Cioglì, A., Molinaro, C., D'Acquarica, I., Kocergin, J., Szczerba, T., Ritchie, H., Villani, C., Gasparrini, F., Introducing enantioselective ultrahigh-pressure liquid chromatography (eUHPLC): theoretical inspections and ultrafast separations on a new sub-2-μm Whelk-O1 stationary phase. Anal. Chem. 2012, 84, 6805-6813

[15]   Pirkle, W. H., Welch, C. J., Lamm, B., Design, synthesis, and evaluation of an improved enantioselective naproxen selector. The Journal of Organic Chemistry. 1992, 57, 3854-3860.10.1021/jo00040a026

[16]   Sciascera, L., Ismail, O., Cioglì, A., Kotoni, D., Cavazzini, A., Botta, L., Szczerba, T., Kocergin, J., Villani, C., Gasparrini, F., Expanding the potential of chiral chromatography for high-throughput screening of large compound libraries by means of

sub–2μm Whelk-O 1 stationary phase in supercritical fluid conditions. Journal of Chromatography A. 2015, 1383, 160-168.10.1016/j.chroma.2015.01.042

[17]   Gonçalves, L., Cravo, S., Fernandes, C., Tiritan, M. E., Development and evaluation of Pirkle-type chiral stationary phase for flash chromatography. Journal of Chromatography A. 2022, 1675, 463156

[18]   Lahiri, S., Thompson, J. L., Moore, J. S., Solvophobically driven π-stacking of phenylene ethynylene macrocycles and oligomers. Journal of the American Chemical Society. 2000, 122, 11315-11319

[19]   Ismail, O. H., Pasti, L., Ciogli, A., Villani, C., Kocergin, J., Anderson, S., Gasparrini, F., Cavazzini, A., Catani, M., Pirkle-type chiral stationary phase on core–shell and fully porous particles: are superficially porous particles always the better choice toward ultrafast high-performance enantioseparations? Journal of Chromatography A. 2016, 1466, 96-104

[20]   Mazzoccanti, G., Manetto, S., Ciogli, A., Villani, C., Gasparrini, F., A perspective on enantioselective chromatography by comparing ultra-high performance supercritical fluid chromatography and normal-phase liquid chromatography through the use of a Pirkle-type stationary phase. TrAC, Trends Anal. Chem. 2022, 147, 116511

[21]   Martin, A. J., Synge, R. L., A new form of chromatogram employing two liquid phases: A theory of chromatography. 2. Application to the micro-determination of the higher monoamino-acids in proteins. Biochemical Journal. 1941, 35, 1358

[22]   Deemter, J. v., Zuiderweg, F., Klinkenberg, A. v., Longitudinal diffusion and resistance to mass transfer as causes of nonideality in chromatography. Chem. Eng. Sci. 1956, 5, 271-289

[23]   Gritti, F., Guiochon, G., The van Deemter equation: Assumptions, limits, and adjustment to modern high performance liquid chromatography. Journal of Chromatography A. 2013, 1302, 1-13

[24]   Johnson, G. J., Encyclopedia of Analytical Science. Reference Reviews. 2005, 19, 38-39

[25]   Wahab, M. F., Armstrong, D., Patel, D. C., Peak shapes and their measurements: the need and the concept behind total peak shape analysis. LCGC Europe. 2017, 30, 670–678-670–678

[26]   Felinger, A., Deconvolution of overlapping skewed peaks. Anal. Chem. 1994, 66, 3066-3072

[27]   Davis, J. M., Giddings, J. C., Statistical theory of component overlap in multicomponent chromatograms. Anal. Chem. 1983, 55, 418-424

[28]   Lundeen, J. T., Juvet, R. S., Quantitative resolution of severely overlapping chromatographic peaks. Anal. Chem. 1981, 53, 1369-1372

[29]   McWilliam, I., Bolton, H., Instrumental peak distortion. III. Analysis of overlapping curves. Anal. Chem. 1971, 43, 883-890

[30]   Handlovic, T. T., Wahab, M. F., Armstrong, D. W., Symmetrization of Peaks in Chiral Chromatography with an Area-Invariant Resolution Enhancement Method. Anal. Chem. 2022, 94, 16638-16646

[31]   Softare, S., PeakFit. 1999.

[32]   Fornstedt, T., Zhong, G., Bensetiti, Z., Guiochon, G., Experimental and theoretical study of the adsorption behavior and mass transfer kinetics of propranolol enantiomers on cellulase protein as the selector. Anal. Chem. 1996, 68, 2370-2378

[33]   Cherrak, D. E., Khattabi, S., Guiochon, G., Adsorption behavior and prediction of the band profiles of the enantiomers of 3-chloro-1-phenyl-1-propanol: Influence of the mass transfer kinetics. Journal of Chromatography A. 2000, 877, 109-122

[34]   Desmet, G., Broeckhoven, K., Extra-column band broadening effects in contemporary liquid chromatography: Causes and solutions. TrAC, Trends Anal. Chem. 2019, 119, 115619

[35]   Kirkland, J., Yau, W., Stoklosa, H., Dilks Jr, C., Sampling and extra-column effects in high-performance liquid chromatography; influence of peak skew on plate count calculations. J. Chromatogr. Sci. 1977, 15, 303-316

[36]   Foley, J. P., Dorsey, J. G., Equations for calculation of chromatographic figures of merit for ideal and skewed peaks. Anal. Chem. 1983, 55, 730-737

[37]   Guiochon, G., Gritti, F., Shell particles, trials, tribulations and triumphs. Journal of Chromatography A. 2011, 1218, 1915-1938

[38]   Gritti, F., Leonardis, I., Shock, D., Stevenson, P., Shalliker, A., Guiochon, G., Performance of columns packed with the new shell particles, Kinetex-C18. Journal of Chromatography A. 2010, 1217, 1589-1603

[39]   Fekete, S., Oláh, E., Fekete, J., Fast liquid chromatography: the domination of core–shell and very fine particles. Journal of chromatography A. 2012, 1228, 57-71

[40]   Fornstedt, T., Forssén, P., Westerlund, D., System peaks and their impact in liquid chromatography. TrAC, Trends Anal. Chem. 2016, 81, 42-50

[41]   Bobály, B., Beck, A., Fekete, J., Guillarme, D., Fekete, S., Systematic evaluation of mobile phase additives for the LC–MS characterization of therapeutic proteins. Talanta. 2015, 136, 60-67

[42]   Blackwell, J. A., Stringham, R. W., Weckwerth, J. D., Effect of mobile phase additives in packed-column subcritical and supercritical fluid chromatography. Anal. Chem. 1997, 69, 409-415

[43]   Pirkle, W., Readnour, R., The influence of end-capping on the enantioselectivity of a chiral phase. Chromatographia. 1991, 31, 129-132

[44]   Delley, R., Series for the exponentially modified Gaussian peak shape. Anal. Chem. 1985, 57, 388-388

[45]   Gelman, A., Analysis of variance—why it is more important than ever. 2005,

[46]   Van Deemter, J., Zuiderweg, F., Klinkenberg, A. v., Longitudinal diffusion and resistance to mass transfer as causes of nonideality in chromatography. Chem. Eng. Sci. 1956, 5, 271-289

[47]   Fallas, M. M., Hadley, M. R., McCalley, D. V., Practical assessment of frictional heating effects and thermostat design on the performance of conventional (3 μm and 5 μm) columns in reversed-phase high-performance liquid chromatography. Journal of Chromatography A. 2009, 1216, 3961-3969

[48]   Handlovic, T. T., Wahab, M. F., Cole, H. D., Alatrash, N., Ramasamy, E., MacDonnell, F. M., McFarland, S. A., Armstrong, D. W., Insights into enantioselective separations of ionic metal complexes by sub/supercritical fluid chromatography. Anal. Chim. Acta. 2022, 1228, 340156